Title

p-y Plasticity Model for Nonlinear Dynamic Analysis of Piles in Liquefiable Soil

Journal

Journal of Geotechnical and Geoenvironmental Engineering, 139(8)

ISSN

1090-0241

Authors

Brandenberg, Scott J
Zhao, Minxing
Boulanger, Ross W
et al.

Publication Date

2013-08-01

DOI

10.1061/(asce)gt.1943-5606.0000847

Peer reviewed

http://dx.doi.org/10.1061/(ASCE)GT.1943-5606.0000847

p-y Plasticity Model for Nonlinear Dynamic Analysis of Piles in Liquefiable Soil

by, Scott J. Brandenberg, M.ASCE[1], Minxing Zhao[2], Ross W. Boulanger, M.ASCE[3], and Daniel W. Wilson, M.ASCE[4]

Abstract

Liquefiable soil-structure interaction material models are developed and implemented in the open-source finite element modeling platform, OpenSees. Inputs to the free-end of the p-y materials include the ground motion and mean effective stress time series from a free-field soil column. Example simulations using a single p-y element attached to a soil element demonstrate key features. The models are then used to analyze centrifuge experiments of a single pile in a level liquefiable profile, and a six-pile group in a sloping liquefiable profile that resulted in lateral spreading. Measured displacements and mean effective stress time series are utilized as inputs to isolate the response of the material models from predictive uncertainties in free-field ground motion and excess pore pressure. The predicted pile response agrees reasonably well with measurements. The cyclic mobility behavior of sand in undrained loading is shown to be an important mechanism affecting bending moments in the piles; neglecting the dilatancy component of the sand's response (i.e., ignoring the cyclic mobility behavior) can result in under-prediction of the demands imposed on the piles.

CE Database subject headings: Soil liquefaction; Pile lateral loads; Plasticity; Centrifuge models; Dynamic analysis.

[1] Associate Professor, 5731 Boelter Hall, Department of Civil and Environmental Engineering, University of California, Los Angeles, 90095-1593 (corresponding author). email: sjbrandenberg@ucla.edu
[2] Graduate Student, Department of Civil and Environmental Engineering, University of California, Los Angeles.
[3] Professor, Department of Civil and Environmental Engineering, University of California, Davis.
[4] Associate Director, Center for Geotechnical Modeling, University of California, Davis.

Introduction

Liquefaction has damaged many pile foundations in past earthquakes, resulting in significant research into the fundamental loading mechanisms. Research studies include centrifuge modeling (e.g., Abdoun et al. 2003, Wilson et al. 2000, Brandenberg et al. 2005, Haigh and Madabhushi 2011), 1-g shake table testing (e.g., Tokimatsu and Suzuki 2004), full-scale field testing using blast-induced liquefaction (e.g., Ashford et al. 2004), and numerical simulations (e.g., Iai 2002). Among the important findings from these studies are: (1) liquefied sand provides some non-zero lateral resistance to piles, and the p-y behavior often exhibits a concave-upward trend that is similar to the undrained stress-strain cyclic mobility response of sand due to dilatancy (Wilson et al. 2000, Rollins et al. 2005), (2) loads from a nonliquefiable laterally spreading crust layer often dominate pile foundation response (e.g., Dobry et al. 2003) and significantly larger deformations are required to mobilize passive resistance compared with nonliquefied soil profiles (Brandenberg et al. 2007a), (3) kinematic demands induced by lateral spreading ground deformation can act simultaneously with inertia demands imposed by a superstructure and pile cap (Boulanger et al. 2007), and (4) static beam on nonlinear Winkler foundation (BNWF) analyses can provide reasonable predictions of bending moments and pile deformations provided that the inputs are carefully selected (e.g., Juirnarongrit and Ashford 2006, Brandenberg et al. 2007b).

The primary benefits of static BNWF simulations are that they can capture many of the salient features of the loading mechanisms, and can be easily performed using commercially available software (e.g., LPile, Reese et al. 2004). The disadvantages are that assumptions must be made regarding the appropriate combination of kinematic and inertia demands, and static simulations cannot reasonably capture the evolution of pile demands as the soil transitions from non-liquefied to liquefied, nor the cyclic mobility behavior following liquefaction. Dynamic simulations have become routine for structures founded on nonliquefiable soils, yet dynamic simulations are quite rare for liquefiable sites simply

because well-vetted tools for performing such simulations are not readily available, and numerical approaches can be computationally expensive. There is a clear need for development and documentation of relatively simple computational tools that permit dynamic analysis of structures at liquefiable sites.

This paper formulates dynamic liquefiable soil-structure interaction materials (i.e., p-y and t-z) that are implemented in a BNWF framework and compared with results from two dynamic centrifuge model tests of pile systems in liquefiable soil profiles, with and without lateral spreading. While the material models described herein have been implemented in OpenSees and used in a number of dynamic numerical studies, their basic formulation and initial examination of their performance have not been previously presented in the literature. This paper therefore presents the mathematical formulation of the material models, followed by a description of the centrifuge models and the analyses of the pile responses using the BNWF method.

PySimple1 Material

Formulation of the PySimple1 material was first presented by Boulanger et al. (1999) and compared with centrifuge model results for piles in soft clay. This material forms the basis for the liquefiable p-y material, PyLiq1, and the PySimple1 equations are presented first. The equations used to describe p-y behavior were chosen as a versatile means of approximating established p-y relations, and are structured for implementation in a displacement-based finite element code. The nonlinear p-y behavior is conceptualized as consisting of elastic ($p\text{-}y^e$), plastic ($p\text{-}y^p$), and gap ($p\text{-}y^g$) components in series (Fig. 1). A dashpot is placed in parallel with the elastic component to model radiation damping. This formulation is consistent with the observation that radiation damping consists largely of elastic wave propagation in

65 the far-field, whereas hysteretic damping dominates the near-field response. The gap component
66 consists of a drag (p^d-y^g) and closure (p^c-y^g) element in parallel. Note that $p = p^c+p^d$, and $y = y^e + y^p + y^g$.

67 *Elastic and-Plastic Components*

68 The elastic component consists of an elastic material with stiffness K^e in parallel with a dashpot to
69 model radiation damping. Force in the elastic component is $p = K^e y^e$, where y^e is the elastic component
70 of displacement. The elastic component is placed in series with a plastic component such that the force,
71 p, in these components is equal. The force in the plastic component is defined on the right side of Eq. 1,
72 where y^p is the plastic component of displacement, C and n are model constants that control the shape
73 of the plastic component, y_{50} is the displacement where $p = 0.5p_{ult}$, and p_o and y_o^p are the values of p
74 and plastic displacement, respectively, at the start of the current plastic loading cycle.

$$p = K^e y^e = p_{ult} - \left(p_{ult} - p_o\right)\left(\frac{C \cdot y_{50}}{C \cdot y_{50} + \left|y^p - y_o^p\right|}\right)^n \tag{1}$$

75

76 The yield function is defined in Eq. 2, where p_{ult} is the ultimate strength, $C_r \cdot p_{ult}$ is the yield stress, and p_α
77 is the back stress (i.e., the value of p at the center of the elastic region). A kinematic hardening law
78 defines evolution of the back stress such that $\dot{p}_\alpha = \dot{p}$ for a plastic loading increment, and $\dot{p}_\alpha = 0$ for an
79 elastic loading increment. The plastic modulus is defined in Eq. 3.

$$f = \left|p - p_\alpha\right| - \left(C_r \cdot p_{ult}\right) \le 0 \tag{2}$$

$$K^p = \frac{\partial p}{\partial y^p} = \frac{n \cdot sign(\dot{y}) \cdot \left(p_{ult} - p_o\right)}{\left|y^p - y_o^p\right| + c \cdot y_{50}}\left(\left[\frac{c \cdot y_{50}}{\left|y^p - y_o^p\right| + c \cdot y_{50}}\right]^n\right) \tag{3}$$

80

Material constants C, n, and C_r define the shape of the backbone curve of the PySimple1 material, and have been adjusted to fit the functional form suggested by Matlock (1970) for piles in clay (C=10, n=5, C_r=0.35), and API (1993) for piles in sand (C=0.5, n=2, C_r=0.2).

Gap Component

The gap component consists of a nonlinear drag element in parallel with a nonlinear closure element such that $p^d + p^c = p$, and the displacement across the gap element is y^g. Force in the drag component, p^d, and closure component, p^c, are defined by Eqs. 4 and 5, respectively, where C_d is a material constant, and p_o^d and y_o^g are the force and plastic gap displacement in the component at the start of the current plastic loading cycle. Evolution of the gap follows logic similar to that of Matlock et al. (1978) with y_o^+ equal to the maximum past value of $y^e + 1.5y_{50}$ and y_o^- equal to the maximum past value of $y^e - 1.5y_{50}$, where $1.5y_{50}$ represents some rebounding of the gap. The tangent modulus for the gap component, K^g, is defined in Eq. 6.

$$p^d = C_d \cdot p_{ult} - \left(C_d \cdot p_{ult} - p_o^d\right)\left[\frac{y_{50}}{y_{50} + 2\left|y^g - y_o^g\right|}\right]^n \tag{4}$$

$$p^c = 1.8 \cdot p_{ult}\left[\frac{y_{50}}{y_{50} + 50\left(y_o^+ - y^g\right)} - \frac{y_{50}}{y_{50} + 50\left(y_o^- - y^g\right)}\right] \tag{5}$$

$$K^g = \frac{\partial p}{\partial y^g} = \frac{2n\left(p_o^d - C_d p_{ult}\right)}{y_{50} + 2\left|y^g - y_o^g\right|}\left(\frac{y_{50}}{y_{50} + 2\left|y^g - y_o^g\right|}\right)^n + \frac{1.8p_{ult}\dfrac{y_{50}}{50}}{\left(\dfrac{y_{50}}{50} - y^g + y_o^+\right)^2} - \frac{1.8p_{ult}\dfrac{y_{50}}{50}}{\left(\dfrac{y_{50}}{50} - y^g + y_o^-\right)^2} \tag{6}$$

Combined Material

Example behavior for the combined material is shown in Fig. 1 for the second cycle of sinusoidal displacement-controlled loading with amplitude equal to $10y_{50}$. Values of C_d = 0.1, 1.0, and 10.0 are shown in the figure and radiation damping is zero for all cases. The material with C_d=0.1 is pinched in the middle, clearly exhibiting behavior that is consistent with a pile moving through an open gap (e.g., Matlock 1970). Resistance in the open gap arises from friction along the sides of the pile. The force amplitude abruptly increases when the gap closes. The material with C_d=10.0 essentially removes the gap component from the material by making it rigid (notice the essentially rigid response in Fig. 1e).

The tangent modulus for the combined material, K, is defined as $K = (1/K^e + 1/K^p + 1/K^g)^{-1}$. The consistent tangent operator is equal to the elasto-plastic tangent modulus for one dimensional problems, and is important to preserve the quadratic rate of asymptotic convergence for iteration schemes commonly used in nonlinear finite element problems (e.g., Simo and Hughes 1998).

PyLiq1 Material

The PyLiq1 material follows the same logic as the PySimple1 material with the only difference being that the capacity of the p-y material, p_{ult_liq}, is treated as a variable that depends on the mean effective stress in the free-field, σ', rather than being specified as a material constant. The value of p_{ult_liq} is degraded as pore pressure develops in the free field, eventually reaching a residual value p_{res} when σ'=0 according to Eq. 7, where σ_o' is the initial free-field effective stress.

$$p_{ult\_liq} = p_{res} + (p_{ult} - p_{res})\frac{\sigma'}{\sigma_o'} \tag{7}$$

This formulation is intended to incorporate the influence of ground shaking and liquefaction on p-y behavior, while retaining some small p-y capacity for the fully-liquefied condition that has been

observed in many model studies (e.g., Wilson et al. 2000, Dobry et al. 2003). The ground motion and mean effective stress are input to the free-ends of the PyLiq1 elements as demonstrated in Fig. 2. These quantities can be obtained from an effective stress site response analysis, though measured quantities are also used as inputs in this paper. The site response simulation can be run separately from the structural analysis, with the recorded outputs written to file and subsequently input to the free-ends of the p-y elements, or it can be run concurrently with the p-y elements and pile part of the same domain as the soil mesh. If run concurrently, the out-of-plane thickness of the soil mesh should be made very large so that an essentially free-field site response condition is achieved (i.e., so that the pile and p-y elements do not affect the site response). The motivation for utilizing free-field motions is that the p-y materials are intended to capture all of the soil-structure-interaction effects, and none of it is modeled by a soil continuum. A three-dimensional continuum with appropriately sized elements near the pile would be required to properly model SSI effects, and such approaches are computationally very expensive for dynamic problems with liquefaction.

In addition to modeling degradation of the p-y behavior as excess pore pressure develops in the free-field, the material is also capable of modeling the transient stiffening associated with the cyclic mobility behavior of sands in cyclic undrained loading. Cyclic mobility behavior is defined as the transition from incrementally contractive to incrementally dilative behavior that is associated with an increase in the tangent stiffness and inverted s-shaped stress-strain behavior. Cyclic mobility significantly influences free-field site response behavior, and this influence is captured as an input to the PyLiq1 material. However, a limitation of the model is that the dilatancy induced by local strains imposed on the soil by the pile can only indirectly be incorporated by specifying an appropriate value for p_{res}. The concave-upward p-y behavior that has been observed in the absence of shaking-induced free-field dilatancy during blast-induced liquefaction studies (Rollins et al. 2005) and in numerical simulations

(e.g., Iai 2002) is not captured by the PyLiq1 formulation. Furthermore, the inverted cone-shaped negative pore pressure region around the pile that was observed by Gonzalez et al. (2009) is not captured by the PyLiq1 material. Assimaki and Varun (2009) formulated a p-y macroelement that links a Bouc-Wen type backbone curve with a pore pressure function that combines free-field pore pressure response with near-field response related to plastic work in the p-y element. This added feature of material behavior requires specification of additional input parameters for the macro-elements. Development of multiple independent models is important for quantifying the effects of epistemic uncertainty.

An illustration of the PyLiq1 material behavior in level ground conditions (i.e., without static shear stress and lateral spreading) is shown in Fig. 3 for a case where a PyLiq1 material with $p_{res}=0.1p_{ult}$ attaches a soil element to a rigid pile. The soil element is modeled as a PressureDependMultiYield02 material using the default input parameters suggested by Yang et al. (2003) for medium dense sand with D_R =50% , and it is subjected to simple shear loading with a cyclic stress ratio of CSR=0.3. The harmonic simple shear stress path is applied at a low enough frequency to render essentially zero inertial stresses. The simulation was performed in OpenSees, with the soil response computed first and the displacements and mean effective stresses from the soil response subsequently imposed on the free end of the p-y element in a separate analysis. This approach ensures that the soil behavior is a free-field input. The excess pore pressure builds up and reaches 1.0 after approximately 6 cycles, and the material behavior is characterized by transient reductions in pore pressure associated with dilatancy. The dilatant tendency at large strains causes sharp increases in the shear stress when the shear strain exceeds the maximum past strain, resulting in the inverted s-shaped stress-strain behavior that characterizes undrained loading of sands. The p-y behavior in the model mimics the stress-strain behavior of the sand

159 in this case and also exhibits an inverted s-shape that is similar to trends observed in centrifuge tests
160 (e.g., Wilson et al. 2000).

161 An illustration of the PyLiq1 material behavior in the presence of lateral spreading is shown in Fig. 4
162 for the same configuration as in Fig. 3, but with a static shear stress imposed on the soil in addition to
163 the cyclic shear stress. Shear strains accumulate in the direction of static shear stress, resulting in
164 permanent deformation of the soil element in a manner that is consistent with lateral spreading. The
165 free-field soil response was input to the same PyLiq1 material as in Fig. 3, but this time the analysis was
166 performed for a rigid pile, and for a flexible pile whose stiffness was adjusted so that the peak pile
167 displacement is equal to $10y_{50}$. The rigid pile attracted large loads during each cycle as the soil spreads
168 past, whereas the flexible pile attracted much smaller loads. The flexible pile deformation is
169 characterized by alternating episodes in which (1) the down-slope movement of the sand is slowed as
170 the sand becomes incrementally dilative, the excess pore pressures reduce, and the sand stiffens, (2) the
171 temporarily stiffened sand exerts greater loads on the pile and displaces it down-slope, (3) the dynamic
172 shear stress on the sand reverses direction, such that the sand becomes incrementally contractive, the
173 excess pore pressures increase again, and the sand softens, and (4) the temporarily softened sand exerts
174 lesser loads on the pile, which allows the pile to rebound in the upslope direction. On the other hand,
175 the rigid pile does not displace downslope during dilatancy cycles, and a much larger load is transmitted
176 to the pile due to the cyclic mobility behavior of the soil. This observation is consistent with centrifuge
177 testing by Haigh (2002) that showed that stiff piles attract much larger lateral spreading loads than
178 flexible piles.

179 In addition to PySimple1 and PyLiq1 for lateral soil-pile interaction, TzSimple1 and TzLiq1 materials
180 were formulated for axial shaft friction, and QzSimple1 was formulated for end bearing resistance.
181 TzSimple1 follows the same logic as PySimple1, except the gapping component is removed, and TzLiq1

follows the same logic as PyLiq1, except the residual capacity of the material is set to zero. The backbone of the TzSimple1 and TzLiq1 materials can be selected to match the relation by Mosher (1984) for axially loaded piles in sand, or by Reese and O'Neill (1987) for drilled shafts. QzSimple1 exhibits a direction-dependent response in which a small uplift capacity can be included to model suction stresses in undrained loading. The backbone of the QzSimple1 material can be selected to match the relation by Reese and O'Neill (1987) for drilled shafts in clay or Vijayvergia (1977) for piles in sand. Including axial interaction can be important for pile groups that rotate in response to lateral loading.

Description of Centrifuge Models

Simulations incorporating the PyLiq1 material are compared with experimental data from centrifuge model CSP2 (Wilson et al. 1997) for single piles in nearly level liquefiable sand, and from model SJB03 (Brandenberg et al. 2005) for pile groups in laterally spreading ground. Model sketches are shown in Fig. 5. Properties of the sand utilized in the studies are summarized in Table 1 for CSP2 and Table 2 for SJB03. Peak friction angles reported in Tables 1 and 2 are estimated based on relative density. Pile properties are summarized in Table 3. Results are presented in prototype units unless otherwise specifically noted.

Model CSP2 consisted of a 0.67m diameter single extended pile shaft embedded 16.8m into a horizontally-layered soil profile consisting of liquefiable loose Nevada sand (D_R=35%) over dense Nevada sand (D_R=75%). Pile groups were also embedded in the model, but only the single pile is studied herein. The single pile was at least 15 diameters from the nearest pile group. A 49 MN mass was attached to the top of the pile at a height of 3.81m above the ground surface. The model was saturated with a pore fluid consisting of water mixed with methylcellulose with a viscosity equal to ten times that of water. Testing

was performed at a centrifugal acceleration of 30*g*. Scaling effects related to pore fluid viscosity are discussed by Wilson et al. (2000).

Model SJB03 consisted of a six-pile group of 1.17m diameter piles embedded into a sloping soil profile consisting of a nonliquefiable overconsolidated crust of San Francisco bay mud over loose Nevada sand (D_R=35%) over dense Nevada sand (D_R=75%). A thin layer of Monterey sand was placed on top of the bay mud to prevent desiccation due to wind currents during spinning. The piles were tied together by an embedded pile cap with length x width x height of 14.2m x 9.2m x 2.2m and mass of 726Mg. A channel was carved in the downslope end of the model to simulate a common geologic condition that results in lateral spreading. The model was saturated with water rather than a viscous pore fluid because some water was squeezed out of the clay into the sand during consolidation on the hydraulic press prior to shaking and this water could not be replaced by viscous pore fluid during saturation. Since the viscosity of the pore fluid was not scaled, the prototype hydraulic conductivity of the sand was 57.2 times higher than for the same water-saturated sand at 1-*g*. The hydraulic conductivity is nevertheless low enough to fully liquefy the sand during shaking. Testing was performed at a centrifugal acceleration of 57.2g.

A sequence of ground motions was imposed on each model, and seven of the ground motions imposed on CSP2 and four of the ground motions imposed on SJB03 are analyzed in this paper. The analyzed motions were scaled versions of the UCSC/Lick Lab, Ch. 1 - 90° strong motion record from the 1989 Loma Prieta earthquake, and the downhole record (depth = 83m) from Port Island during the 1995 Kobe earthquake. The ground motion profile was recorded at discrete points using vertical arrays of horizontal accelerometers, and the acceleration records were double-integrated in time to obtain free-field displacement records. The free-field pore pressure profile was recorded using vertical arrays of piezometers. Test CSP2 consisted of a level ground profile and the permanent component of the soil

displacement was negligible, hence time series of ground displacement could be obtained from double integration of acceleration records. On the other hand, the low frequency component of lateral spreading displacement from SJB03 could not be obtained by integration of acceleration records, but was measured using displacement sensors attached to the nonliquefied crust. The complete ground motion time series, including low frequency and high frequency components of the crust displacement, were computed using complementary filters applied to the accelerometer and displacement sensor records. The low frequency components of the soil displacements below the ground surface were assumed to be proportional to those at the ground surface, and the final displaced shape of the soil profile (as determined from post-test profiles of vertical markers embedded in the model) was used to determine the coefficients of proportionality for those low frequency components. Displacement time series were then computed by combining the low and high frequency components. Validation of this procedure and the selection of appropriate filters for the equipment used in these centrifuge tests are discussed in Kutter and Balakrishnan (1998).

Material Properties for p-y, t-z, and Q-z elements

The capacity of the p-y materials, p_{ult}, was estimated using the API (1993) equations for piles in sand. A p-multiplier approach was to define the residual capacity as $p_{res} = m_p p_{ult}$, where m_p was defined based on Brandenberg (2005). The modulus of subgrade reaction in sand deposits is often assumed to vary linearly with depth, however the elastic modulus for clean sands is known to vary approximately with the square root of confining stress (e.g., Yamada et al. 2008). Hence, a parabolic relation was used to define the elastic stiffness with depth. The crust load acting on the embedded pile cap for test SJB03 was estimated to be 6940kN based on the sum of passive earth pressure and side and base friction summarized by Brandenberg et al. (2005). Pile group effects are considered for the mobilized crust load because clay may become trapped between the piles, thereby causing the pile group to act as an

249 equivalent block (Brandenberg et al. 2005). However, group effects are not included for the sand layers
250 based on tests that show group interaction effects to be negligible in liquefied soils (Rollins et al. 2005).
251 Lateral load transfer between pile groups and nonliquefied crusts was observed to be significantly softer
252 for crusts spreading over liquefied soil compared with nonliquefied soil profiles (Brandenberg et al.
253 2007a). The p-y materials in the nonliquefied crust were therefore adjusted so that the ultimate capacity
254 was mobilized at a relative displacement of 40% of the crust thickness rather than a more typical value
255 of 1 to 7% of the crust thickness observed in load tests in nonliquefied soil profiles.

256 The single-pile for CSP2 required only p-y elements to model lateral load transfer, but the pile group
257 in SJB03 required t-z elements to model shaft friction and Q-z elements to model end bearing since the
258 pile group forms a frame that can rock during lateral loading. The t-z elements were modeled using
259 TzLiq1 materials with $t_{ult}=K_oB\sigma_{vo}'\tan(2/3\phi')$, where $K_o = 1-\sin\phi'$, and σ_{vo}' is the initial vertical effective
260 stress prior to shaking. Horizontal stresses at the soil-pile interface typically increase when closed-ended
261 pipe piles are driven into the soil. However, in this case the piles were driven into the models at 1*g*,
262 therefore significant changes in horizontal pressure are not anticipated. The bearing capacity at the tip
263 of the piles was estimated to be 10MN using bearing factors by Meyerhof (1976), and end bearing
264 resistance was modeled using QzSimple1 materials since there was little excess pore pressure generated
265 in the end bearing stratum in each case.

266 **Numerical Modeling Approach**

267 Numerical models of the pile were constructed in OpenSees (McKenna and Fenves 2001) using 50
268 elements along the length of the pile with p-y elements attached at each node below the ground
269 surface. For CSP2 the piles did not yield during testing, and were therefore modeled as elastic beam
270 column elements with properties summarized in Table 3. A mass was assigned to the top node. For

SJB03, the piles did slightly yield during testing, and were therefore modeled using nonlinear beam column elements. The piles were tied together at their head by a pile cap composed of very stiff (essentially rigid) beam column elements. An elastic rotational element attached the pile head to the pile cap to model the measured rotational stiffness of 1300 MN-m/rad at the connection. Masses were distributed among the pile cap nodes and PyLiq1 materials were attached to the top and bottom of the pile cap. For convenience, PyLiq1 materials were utilized for the nonliquefied crust layer as well as in the liquefiable layers but the recorded mean effective stress time series input to the free-ends of the crust were essentially constant since the clay did not generate significant excess pore pressure during the tests. Hence, the PyLiq1 material response was nearly identical to what the PySimple1 material response would have been. TzLiq1 materials were distributed along the length of the piles and QzSimple1 materials were attached to the pile tips. This configuration permits the pile group to rotate during lateral loading, which is an important feature of the response of laterally loaded pile groups. The free-ends of the t-z and Q-z elements were fixed.

Time series of displacement and mean effective stress were linearly interpolated from the recorded data, and imposed on the free-ends of the p-y elements. Recordings of acceleration and pore pressure were from sensors at least 10 pile diameters from the nearest foundation. In forward predictions, displacements and pore pressures would need to be estimated from a site response simulation. However, in this study the measured inputs are utilized to isolate the response of the PyLiq1 materials so that errors in the p-y elements could be separated from errors in site response simulations. Small-strain damping of approximately 2% in the frequency range of interest was achieved using Rayleigh damping. The convergence tolerance on the norm of the displacement residuals was set to 10^{-6} (using the normDispIncr command), and displacement constraints were enforced using the transformation method (using the Transformation command). The equation of motion was integrated using the Hilbert-

294 Hughes-Taylor integrator (using the HHT command) with α=0.7. The time step was adjusted as needed
295 to facilitate convergence (using the VariableTransient command).

296 **Numerical Results for CSP2**

297 Example analysis results for CSP2 are shown in Fig. 6 for a Santa Cruz motion with a peak base
298 acceleration of 0.42g. The excess pore pressure ratio near the center of the loose sand layer reaches 1.0
299 approximately 5s after the start of strong shaking, and subsequently exhibits modest dilation-induced
300 drops in pore pressure. Excess pore pressure ratios are plotted in the free-field, far away from the pile
301 groups, and also at a location immediately adjacent to the pile. Dilation-induced spikes are apparent in
302 both records, but are slightly more pronounced in the record near the pile, presumably due to the
303 additional increment of dilatancy caused by strains imposed on the near field soil by the pile. The peak
304 bending moment (measured and predicted) is mobilized during one such dilation-induced drop in pore
305 pressure at approximately time = 26s. The bending moment and superstructure acceleration records are
306 predicted quite well. The bending moment record was taken at a depth of approximately 3B, where the
307 peak bending moments were measured. Computed values of subgrade reaction near the center of the
308 loose sand do not agree with measurements as well as computed values of bending moment and
309 superstructure acceleration, but nevertheless, the peak responses are predicted well during critical
310 cycles.

311 The same records from Fig. 6 are plotted in Fig. 7 for a Kobe motion with a peak base acceleration of
312 0.61g. The frequency content of the Kobe motion is significantly lower than the Santa Cruz motion, and
313 the dilatancy response in the liquefied sand in much more pronounced as a result. Once again, the peak
314 bending moment and peak superstructure acceleration occurred during a transient drop in excess pore
315 pressure. The superstructure acceleration reached a peak near 1.5g that was under-predicted by the

316 analyses by about 0.5g, but the computed values track the measured response quite well other than for
317 the one cycle that produced the peak value. The bending moment mobilized in the pile is also predicted
318 reasonably well.

319 Acceleration response spectra were computed for the superstructure motion for three Santa Cruz
320 motions and four Kobe motions of various intensities. The shapes of the spectra tend to agree quite well
321 with measurements. However, for the Santa Cruz motions, the computed values tend to be too high for
322 the high-intensity motions and too low for the low-intensity motions. For the Kobe motions, the
323 disagreements could not be so simply characterized based on input motion intensity. Better agreement
324 could be achieved by adjusting the stiffness of the p-y materials on a motion-specific basis by increasing
325 K_{ref} for the small motions and decreasing K_{ref} for the large motions. This may partly reflect the effect of
326 loading history on p-y behavior, which is not included in the analyses. Another factor may be that the
327 functional form of the API (1993) sand curve is very linear at small values of y, hence there is very little
328 small-strain nonlinearity in the PyLiq1 materials. Varun (2010) also demonstrated that the API curve is
329 too linear, and suggested an alternative form that resulted in better agreement with measurements.

330 **Numerical Results for SJB03**

331 Computed results for SJB03 are compared with measurements for the medium intensity Santa Cruz
332 motion with peak base acceleration of 0.35g in Fig. 9. Some residual loads were present in the pile
333 groups at the end of each motion for SJB03 due to lateral spreading deformations and the motions were
334 applied in sequence in the numerical simulations, which explains the non-zero initial values of some
335 quantities in Fig. 9. The excess pore pressure ratio in the loose sand does not reach 1.0 for this motion
336 even though surface evidence of liquefaction was observed in the form of 0.4m of lateral spreading
337 ground displacement. This may be attributed to the effect that sustained downslope shear stresses has

on limiting values of excess pore pressure ratio (e.g., Ishihara and Nagase 1980). Computed values are reasonably consistent with the measurements for bending moment, crust load, pile cap inertia, and pile cap displacement, though the residual loads on the pile group are larger than predicted.

Computed values for the large Kobe motion with peak base acceleration of 0.67g are shown in Fig. 10. This motion fully liquefied the loose sand in the first cycle of strong shaking, and the response is characterized by very pronounced dilatancy spikes. Each downward spike in the pore pressure record is associated with a local peak in the crust load, a local maximum bending moment amplitude (the largest amplitude bending moments were negative in this case), and a local maximum in pile cap inertia. The measured crust load sometimes exceeded the predicted maximum crust load, and as a result the peak bending moments were slightly under-predicted in the analysis. Nevertheless, agreement between the measured and predicted responses is quite reasonable.

Response spectra for the pile cap motion are shown in Fig. 11. The shape of the spectra was reasonably predicted in each case, though the amplitude was not predicted perfectly. Once again, the small-strain stiffness of the p-y materials could be adjusted to provide a better prediction of pile cap motion (results not shown for brevity), which may either represent the effects of loading history not being accounted for in the analyses or indicate a need for a p-y material functional form that more correctly captures small-strain nonlinearity.

Discussion

A key feature of the PyLiq1 material is that it incorporates not only the development of excess pore pressure during cyclic loading, but also transient reductions in pore pressure caused by dilatancy. Dilatancy was shown to be an important driver of peak bending moments in the pile foundations from centrifuge studies by Wilson et al. (2000) and Brandenberg et al. (2005). This paper input the measured

360 pore pressures; hence the dilatancy response was included to the extent it was measured in the free-
361 field during a particular motion. However, the pore pressure response would need to be numerically
362 simulated in a forward analysis. Advanced plasticity models are capable of capturing the dilatancy
363 response (e.g., Dafalias and Manzari 2004; Yang et al. 2003, Boulanger and Ziotopoulou, 2012) whereas
364 other models can capture the development of excess pore pressure but not the transient reductions
365 caused by dilatancy (e.g., Martin and Qiu 2001, Hashash 2011). To explore the influence of dilatancy on
366 pile response, simulations for the single pile from CSP2 were repeated with the same displacement
367 records input to the free-ends of the p-y materials, but with the measured pore pressure response
368 adjusted so that it only increased (Fig. 12). The motions in Fig. 12 were selected because in both cases
369 the loose sand fully liquefied, but the extent of the post-liquefaction dilatancy-induced drops in pore
370 pressure were quite different. The Santa Cruz motion exhibited very small pore pressure drops whereas
371 the Kobe motion exhibited very pronounced drops.

372 For the Santa Cruz motion, the simulation with the always-increasing pore pressure record is very
373 similar to the simulation that utilized the measured pore pressure input. On the other hand, significant
374 differences arise for the Kobe motion, where the always-increasing pore pressure response resulted in a
375 significantly smaller prediction of peak bending moments and superstructure acceleration (Table 4).
376 These cases demonstrate that dilatancy can be a significant factor that drives the critical loading cycles
377 for piles in liquefied ground. Similar conclusions were reached in previous studies that utilized an always
378 increasing pore pressure response to model the single pile by Wilson (2000). Liyanapathirana and Poulos
379 (2005) analyzed the Kobe motion, and found that bending moments were under-predicted following
380 liquefaction. Finn et al. (2000) analyzed the Santa Cruz motion, and found that bending moments were
381 reasonably predicted. Similarly, Kramer et al. (2011) and Ziotopoulou et al. (2011) illustrate that

dilatancy is an important factor in obtaining reasonable ground motion simulations of the seismic responses of liquefying soil profiles.

The cases studied in this paper involved liquefaction of loose sands. Wilson et al. (2000) studied liquefaction potential of medium dense sands and found them to be more dilatant and exhibit more pronounced cyclic mobility behavior compared with the looser sands. Analysis of a medium dense sand case is presented by Boulanger et al. (2004).

Conclusions

Static methods for analyzing piles in liquefied ground are appropriate for many structures for which dynamic simulations are too complex and costly, and uncertainties inherent to static analysis approaches can be accommodated by adequate conservatism. However, dynamic simulations may be warranted for important structures, and may be required for complex structures for which liquefaction-compatible inertia demands are difficult to quantify without performing a dynamic simulation. Advancing beyond equivalent static analysis of piles in liquefied ground requires development of robust, validated numerical tools for performing dynamic simulations. This paper addresses this need by formulating liquefiable soil-structure interaction elements that utilize free-field site response quantities as inputs.

Comparisons with centrifuge test data show that the materials can reasonably capture key features of dynamic response when measured displacements and excess pore pressures are utilized as inputs. Forward predictions would require a site response simulation to obtain ground motion and effective stress time series to input to the p-y model, which introduces additional uncertainty to the predictions. The measured inputs were utilized instead of a site response prediction in this study to isolate the behavior of the p-y materials.

Cyclic mobility behavior that is associated with inverted s-shaped stress strain behavior during undrained loading of sands also causes inverted s-shaped p-y behavior for piles embedded in liquefied sand. Cyclic mobility behavior was found to be the mechanism responsible for mobilization of the peak bending moments in the piles presented in this study. Simulations that neglected cyclic mobility behavior (i.e., by inputting an always-increasing pore pressure response) under-predicted bending moments and superstructure accelerations compared with measurements, and compared with simulations that included cyclic mobility behavior. Therefore, neglecting the influence of cyclic mobility on pile response could result in unconservative predictions and unforeseen damage or failure.

Acknowledgments

Funding for this work was provided by Caltrans and the National Science Foundation through the Pacific Earthquake Engineering Research Center. The contents of this paper do not necessarily represent a policy of either funding agency or endorsement by the state or federal government. The authors would like to thank Christina Curras for doing the initial model development work on the p-y material models prior to their implementation in OpenSees. Tom Shantz provided valuable technical comments and suggestions. The centrifuge shaker was designed and constructed with support from the National Science Foundation (NSF), Obayashi Corp., Caltrans, and the University of California. Upgrades were funded by NSF award CMS-0086566 through the George E. Brown, Jr. Network for Earthquake Engineering Simulation (NEES).

Notation

B = pile diameter

C = modeling constant that contributes to shape of p-y backbone curve

C_r = modeling constant that controls size of elastic region

C_d = modeling constant that controls subgrade reaction load in open gap

CSR = cyclic stress ratio

D_R = relative density

K_o = coefficient of at-rest earth pressure

K = tangent stiffness of p-y element

K^e = tangent stiffness of elastic component

K^p = tangent stiffness of plastic component

K^g = tangent stiffness of gap component

n = modeling constant that contributes to shape of p-y backbone curve

p = subgrade reaction due to relative displacement between soil and pile

p^d = component of subgrade reaction in drag element

p^c = component of subgrade reaction in closure element

p_α = subgrade reaction value at center of elastic region

p_{res} = ultimate resistance of p-y element for fully-liquefied condition (i.e., with r_u=1)

p_{ult} = ultimate resistance of p-y element for non-liquefied condition (i.e., with r_u=0)

p_{ult_liq} = ultimate resistance of p-y element corresponding to $0 < r_u < 1$

p_o = value of subgrade reaction at start of current plastic loading cycle

p_o^d = component of subgrade reaction in drag element at start of current plastic loading cycle

r_u = excess pore pressure ratio

t_{ult} = ultimate shaft friction load per unit pile length

y = relative displacement between soil and pile

y_{50} = relative displacement between soil and pile when half of ultimate load is mobilized in p-y element

y^e = elastic component of relative displacement between soil and pile

y^p = plastic component of relative displacement between soil and pile

y^g = gap component of displacement between soil and pile

y_o^g=value of gap component of relative displacement between soil and pile at start of current plastic loading cycle

453 y_o^p = value of plastic component of relative displacement between soil and pile at start of current plastic
454 loading cycle

455 y_o^+ = gap evolution term equal to maximum past value of y^e+1.5y_{50}

456 y_o^- = gap evolution term equal to maximum past value of y^e-1.5y_{50}

457 ϕ' = peak friction angle

458 σ' = current effective stress in free-field soil

459 σ_o' = initial effective stress in free-field soil

460 σ_{vo}' = vertical effective stress

461

462 **References**

463 Abdoun, T., Dobry, R., O'Rourke, T. D., and Goh, S. H. (2003). ''Pile response to lateral spreads:
464 Centrifuge modeling.'' *J. Geotech. Geoenviron. Eng., ASCE.* 129(10), 869–878.

465 American Petroleum Institute (API). (1993). *Recommended Practice for Planning, Design, and*
466 *Constructing Fixed Offshore Platforms*. API RP 2A - WSD, 20th ed., American Petroleum Institute.

467 Ashford S.A., Rollins, K.M., and Lane, D. (2004). "Blast-Induced Liquefaction for Full-Scale Foundation
468 Testing," Journal of Geotechnical and Geoenvironmental Engineering,ASCE, 130(8), pp. 798-806.

469 Assimaki, D., and Varun. (2009). "Nonlinear Macroelements for Performance-Based Design of Pile-
470 Supported Waterfront Structures in Liquefiable Sites," *Proceedings, International Conference on*
471 *Performance-Based Design in Earthquake Geotechnical Engineering*, Paper No. 253, pp. 1791-1798.
472 T. Kokusho et al., Eds. London: Taylor and Francis Group.

473 Boulanger, R.W., and Ziotopoulou, K. (2012). "A sand plasticity model for earthquake engineering
474 applications: Version 2.0." Report No. UCD/CGM-12-01, Center for Geotechnical Modeling,
475 Department of Civil and Environmental Engineering, University of California, Davis, CA. 101p.

476 Boulanger, R. W., Chang, D., Brandenberg, S. J., Armstrong, R. J., and Kutter, B. L. (2007). "Seismic design
477 of pile foundations for liquefaction effects." Earthquake Geotechnical Engineering, 4th International
478 Conference on Earthquake Geotechnical Engineering – Invited Lectures, K. D. Pitilakis, ed., Springer,
479 The Netherlands, 277-302.
480 Brandenberg, S.J., Boulanger, R.W., Kutter, B.L., and Chang, D. (2005). "Behavior of pile foundations in
481 laterally spreading ground during centrifuge tests." *J. Geotech. Geoenviron. Eng.*, ASCE., 131(11),
482 1378-1391.
483 Brandenberg, S.J., Boulanger, R.W., Kutter, B.L., and Chang, D. (2007a). "Liquefaction-induced softening
484 of load transfer between pile groups and laterally spreading crusts." J. Geotech. Geoenviron. Eng.,
485 ASCE, 133(1). 91-103.
486 Brandenberg, S.J., Boulanger, R.W., Kutter, B.L., and Chang, D. (2007b). “Static pushover analyses of pile
487 groups in liquefied and laterally spreading ground in centrifuge tests.” J. Geotech. Geoenviron. Eng.,
488 ASCE, 133(9), 1055-1066.
489 Dafalias, Y.F., and Manzari, M.T. (2004). "Simple plasticity sand model accounting for fabric change
490 effects." *J. Eng. Mech.* 130(6). 622-364.
491 Dobry, R., Abdoun, T., O’Rourke, T. D., and Goh, S. H. (2003). "Single Piles in Lateral Spreads: Field
492 Bending Moment Evaluation." *J. Geotech. Geoenviron. Eng.,* ASCE, Vol. 129(10), 879-889.
493 Finn, W.D., Thavaraj, T., Wilson, D.W., Boulanger, R.W., and Kutter, B.L. (2000). “Seismic response
494 analysis of pile foundations at liquefiable sites.” Proc. 12th World Conference on Earthquake
495 Engineering, New Zealand, Paper No. 0422.
496 González, L., Abdoun, T., and Dobry, R. (2009). "Effect of soil permeability on centrifuge modeling of pile
497 response to lateral spreading." *J. Geotech. Geoenviron. Eng.*, ASCE, 135(1), 62-73.
498 Haigh, S. K. (2002). "Effects of earthquake-induced liquefaction on pile foundations in sloping ground."
499 Ph.D. dissertation, Cambridge University, UK.

Haigh, S.K. & Madabhushi, S.P.G. (2011) Centrifuge modeling of pile-soil interaction in liquefiable slopes. Geomechanics and Engineering **3**(1) 1-16

Hashash, Y.M.A. (2011). “DEEPSOIL v5.0: User Manual and Tutorial”. Board of Trustees of University of Illinois at Urbana Champaign. 107p.

Iai, S. (2002). "Analysis of soil deformation around a cylindrical rigid body." Proc. U.S.-Japan Seminar on Seismic Disaster Mitigation in Urban Area by Geotechnical Engineering, I. Towhata and R. W. Boulanger, eds., Anchorage, Alaska, June.

Ishihara, K., and Nagase, H. (1980). "Cyclic simple shear tests on saturated sand in multi-directional loading," by Ishihara and Yamazaki (1980). Soils and Foundations, Japanese Society of Soil Mechanics and Foundation Engineering, 20(1), March. Closure to discussion.

Juirnarongrit, T., and Ashford, S.A. (2006). “Soil-Pile Response to Blast-Induced Lateral Spreading. II: Analysis and Assessment of the p-y Method,” Journal of Geotechnical and Geoenvironmental Engineering, ASCE, 132(2), pp. 163-172.

Kramer, S. L., A. J. Hartvigsen, S. S. Sideras, and P. T. Ozener (2011), "Site Response Modeling in Liquefiable Soil Deposits", 4th IASPEI / IAEE Intl. Symposium, Effects of Surface Geology on Seismic Motion, Univ. of California, Santa Barbara, August 23-26.

Kutter, B.L., and Balakrishnan, A. (1998) “Dynamic model test data from electronics to knowledge,” *Proc. Centrifuge ’98*, T. Kimura, O. Kusakabe, and J. Takemura, eds., pp. 931–943, A. A. Balkema Publishers, (Rotterdam, Netherlands).

Liyanapathirana, D.S., and Poulos, H.G. (2005). “Seismic lateral response of piles in liquefying soil.” *J. Geotech. Geoenviron. Eng.*, 131(12), 1466-1479.

Matlock, H. (1970). "Correlations of design of laterally loaded piles in soft clay." *Proc. Offshore Technology Conference*, Houston, TX, Vol 1, No.1204, pp. 577-594.

Matlock, H., Foo, S. H., and Bryant, L. L. (1978). ‘‘Simulation of lateral pile behavior.’’ *Proc., Earthquake Engrg. and Soil Dyn.*, ASCE, New York, 600–619.

McKenna, F., and Fenves, G.L. (2001). "OpenSees Manual." PEER Center, http://OpenSees.berkeley.edu.

Martin, G.R., and Qiu, P. (2001), “Site Liquefaction Evaluation: The Application of Effective Stress Site Response Analyses,” draft technical report prepared for the Multidisciplinary Center for Earthquake Engineering Research, Buffalo, NY.

Mosher, R.L. (1984). "Load Transfer Criteria for Numerical Analysis of Axial Loaded Piles in Sand." US Army Engineering Waterways Experimental Station, Automatic Data Processing Center, Vicksburg, Mississippi, January.

Reese, L. C. and M. W. O'Neill. (1987). "Drilled Shafts: Construction Procedures and Design Methods." Report No. FHWA-HI-88-042, U.S. Department of Transportation, Federal Highway Administration, Office of Implementation, McLean, Virginia.

Reese, L. C., Wang, S. T., Isenhower, W. M., Arrelaga, J.A., and Hendrix, J. A. (2000). *LPILE Plus Verion 4.0m,* Ensoft, Inc. Austin, TX.

Rollins, K.M., Gerber, T.M., Lane, J.D. and Ashford. S.A. (2005). "Lateral Resistance of a Full-Scale Pile Group in Liquefied Sand." J. Geotechnical and Geoenvironmental Engrg., ASCE, Vol. 131, No. 1, p. 115-125.

Simo, J.C., and Hughes T.J.R. (1998). Computational Inelasticity. Springer, New York. 392 p.

Tokimatsu, K. and Suzuki, H. (2004). "Pore water pressure response around pile and its effects on p-y behavior during soil liquefaction." Soils and Foundations, 44(6), 101-110.

Vijayvergiya, V. N. (1977). "Load-Movement Characteristics of Piles." Proceedings, Ports 77 Conference, American Society of Civil Engineers, Long Beach, California, March.

Wilson, D.W., Boulanger, R.W., and Kutter, B.L. (1997). "Soil-pile-superstructure interaction at soft or liquefiable soils sites - centrifuge data report for CSP2." UCD/CGMDR-97/03. University of California, Davis.

Wilson, D. W., Boulanger, R. W., and Kutter, B. L. (2000). "Seismic lateral resistance of liquefying sand." *J. Geotech. Geoenviron. Eng.*, ASCE, 126(10): 898-906.

Yamada, S., Hyodo, M., Orense, R.P., Dinesh, S.V., and Hyodo, T. (2008). "Strain-dependent dynamic properties of remolded sand-clay mixtures." *J. Geotech. Geoenviron. Eng.*, 134(7), 972-981.

Yang, Z., Elgamal, A., and Parra, E., (2003). "A Computational Model for Liquefaction and Associated Shear Deformation," *Journal of Geotechnical and Geoenvironmental Engineering*, ASCE, Vol. 129, No. 12.

Ziotopoulou, K., Boulanger, R. W., and Kramer, S. L. (2012). "Site response analysis of liquefying sites." Proceedings, Geocongress 2012, ASCE, Oakland, CA.

p-y Plasticity Model for Nonlinear Dynamic Analysis of Piles in Liquefiable Soil

by, Scott J. Brandenberg, M.ASCE[1], Minxing Zhao[2], Ross W. Boulanger, M.ASCE[3], and Daniel W. Wilson, M.ASCE[4]

Abstract

Liquefiable soil-structure interaction material models are developed and implemented in the open-source finite element modeling platform, OpenSees. Inputs to the free-end of the p-y materials include the ground motion and mean effective stress time series from a free-field soil column. Example simulations using a single p-y element attached to a soil element demonstrate key features. The models are then used to analyze centrifuge experiments of a single pile in a level liquefiable profile, and a six-pile group in a sloping liquefiable profile that resulted in lateral spreading. Measured displacements and mean effective stress time series are utilized as inputs to isolate the response of the material models from predictive uncertainties in free-field ground motion and excess pore pressure. The predicted pile responses agree reasonably well with measurements. The cyclic mobility behavior of sand in undrained loading is shown to be an important mechanism affecting bending moments in the piles; neglecting the dilatancy component of the sand's response (i.e., ignoring the cyclic mobility behavior) can result in under-prediction of the demands imposed on the piles.

CE Database subject headings: Soil liquefaction; Pile lateral loads; Plasticity; Centrifuge models; Dynamic analysis.

[1] Associate Professor, 5731 Boelter Hall, Department of Civil and Environmental Engineering, University of California, Los Angeles, 90095-1593 (corresponding author). email: sjbrandenberg@ucla.edu
[2] Graduate Student, Department of Civil and Environmental Engineering, University of California, Los Angeles.
[3] Professor, Department of Civil and Environmental Engineering, University of California, Davis.
[4] Associate Director, Center for Geotechnical Modeling, University of California, Davis.

Introduction

Liquefaction has damaged many pile foundations in past earthquakes, resulting in significant research into the fundamental loading mechanisms. Research studies include centrifuge modeling (e.g., Abdoun et al. 2003, Wilson et al. 2000, Brandenberg et al. 2005, Haigh and Madabhushi 2011), 1-g shake table testing (e.g., Tokimatsu and Suzuki 2004), full-scale field testing using blast-induced liquefaction (e.g., Ashford et al. 2004), and numerical simulations (e.g., Iai 2002). Among the important findings from these studies are: (1) liquefied sand provides some non-zero lateral resistance to piles, and the p-y behavior often exhibits a concave-upward trend that is similar to the undrained stress-strain cyclic mobility response of sand due to dilatancy (Wilson et al. 2000, Rollins et al. 2005), (2) loads from a nonliquefiable laterally spreading crust layer often dominate pile foundation response (e.g., Dobry et al. 2003) and significantly larger deformations are required to mobilize passive resistance compared with nonliquefied soil profiles (Brandenberg et al. 2007a), (3) kinematic demands induced by lateral spreading ground deformation can act simultaneously with inertia demands imposed by a superstructure and pile cap (Boulanger et al. 2007), and (4) static beam on nonlinear Winkler foundation (BNWF) analyses can provide reasonable predictions of bending moments and pile deformations provided that the inputs are carefully selected (e.g., Juirnarongrit and Ashford 2006, Brandenberg et al. 2007b).

The primary benefits of static BNWF simulations are that they can capture many of the salient features of the loading mechanisms, and can be easily performed using commercially available software (e.g., LPile, Reese et al. 2004). The disadvantages are that assumptions must be made regarding the appropriate combination of kinematic and inertia demands, and static simulations cannot reasonably capture the evolution of pile demands as the soil transitions from non-liquefied to liquefied, nor the cyclic mobility behavior following liquefaction. Dynamic simulations have become routine for structures founded on nonliquefiable soils, yet dynamic simulations are quite rare for liquefiable sites simply

because well-vetted tools for performing such simulations are not readily available, and numerical approaches can be computationally expensive. There is a clear need for development and documentation of relatively simple computational tools that permit dynamic analysis of structures at liquefiable sites.

This paper formulates dynamic liquefiable soil-structure interaction materials (i.e., p-y and t-z) that are implemented in a BNWF framework and compared with results from two dynamic centrifuge model tests of pile systems in liquefiable soil profiles, with and without lateral spreading. While the material models described herein have been implemented in OpenSees and used in a number of dynamic numerical studies, their basic formulation and initial examination of their performance have not been previously presented in the literature. This paper therefore presents the mathematical formulation of the material models, followed by a description of the centrifuge models and the analyses of the pile responses using the BNWF method.

PySimple1 Material

Formulation of the PySimple1 material was first presented by Boulanger et al. (1999) and compared with centrifuge model results for piles in soft clay. This material forms the basis for the liquefiable p-y material, PyLiq1, and the PySimple1 equations are presented first. The equations used to describe p-y behavior were chosen as a versatile means of approximating established p-y relations, and are structured for implementation in a displacement-based finite element code. The nonlinear p-y behavior is conceptualized as consisting of elastic ($p\text{-}y^e$), plastic ($p\text{-}y^p$), and gap ($p\text{-}y^g$) components in series (Fig. 1). A dashpot is placed in parallel with the elastic component to model radiation damping. This formulation is consistent with the observation that radiation damping consists largely of elastic wave propagation in

65 the far-field, whereas hysteretic damping dominates the near-field response. The gap component
66 consists of a drag (p^d-y^g) and closure (p^c-y^g) element in parallel. Note that $p = p^c+p^d$, and $y = y^e + y^p + y^g$.

67 *Elastic and-Plastic Components*

68 The elastic component consists of an elastic material with stiffness K^e in parallel with a dashpot to
69 model radiation damping. Force in the elastic component is $p = K^e y^e$, where y^e is the elastic component
70 of displacement. The elastic component is placed in series with a plastic component such that the force,
71 p, in these components is equal. The force in the plastic component is defined on the right side of Eq. 1,
72 where y^p is the plastic component of displacement, C and n are model constants that control the shape
73 of the plastic component, y_{50} is the displacement where $p = 0.5p_{ult}$, and p_o and y_o^p are the values of p
74 and plastic displacement, respectively, at the start of the current plastic loading cycle.

$$p = K^e y^e = p_{ult} - \left(p_{ult} - p_o\right)\left(\frac{C \cdot y_{50}}{C \cdot y_{50} + \left|y^p - y_o^p\right|}\right)^n \tag{1}$$

75

76 The yield function is defined in Eq. 2, where p_{ult} is the ultimate strength, $C_r \cdot p_{ult}$ is the yield stress, and p_α
77 is the back stress (i.e., the value of p at the center of the elastic region). A kinematic hardening law
78 defines evolution of the back stress such that $\dot{p}_\alpha = \dot{p}$ for a plastic loading increment, and $\dot{p}_\alpha = 0$ for an
79 elastic loading increment. The plastic modulus is defined in Eq. 3.

$$f = \left|p - p_\alpha\right| - \left(C_r \cdot p_{ult}\right) \le 0 \tag{2}$$

$$K^p = \frac{\partial p}{\partial y^p} = \frac{n \cdot sign(\dot{y}) \cdot \left(p_{ult} - p_o\right)}{\left|y^p - y_o^p\right| + c \cdot y_{50}}\left(\left[\frac{c \cdot y_{50}}{\left|y^p - y_o^p\right| + c \cdot y_{50}}\right]^n\right) \tag{3}$$

80

Material constants C, n, and C_r define the shape of the backbone curve of the PySimple1 material, and have been adjusted to fit the functional form suggested by Matlock (1970) for piles in clay (C=10, n=5, C_r=0.35), and API (1993) for piles in sand (C=0.5, n=2, C_r=0.2).

Gap Component

The gap component consists of a nonlinear drag element in parallel with a nonlinear closure element such that $p^d + p^c = p$, and the displacement across the gap element is y^g. Force in the drag component, p^d, and closure component, p^c, are defined by Eqs. 4 and 5, respectively, where C_d is a material constant, and p_o^d and y_o^g are the force and plastic gap displacement in the component at the start of the current plastic loading cycle. Evolution of the gap follows logic similar to that of Matlock et al. (1978) with y_o^+ equal to the maximum past value of $y^e + 1.5y_{50}$ and y_o^- equal to the maximum past value of $y^e - 1.5y_{50}$, where $1.5y_{50}$ represents some rebounding of the gap. The tangent modulus for the gap component, K^g, is defined in Eq. 6.

$$p^d = C_d \cdot p_{ult} - \left(C_d \cdot p_{ult} - p_o^d\right)\left[\frac{y_{50}}{y_{50} + 2\left|y^g - y_o^g\right|}\right]^n \tag{4}$$

$$p^c = 1.8 \cdot p_{ult}\left[\frac{y_{50}}{y_{50} + 50\left(y_o^+ - y^g\right)} - \frac{y_{50}}{y_{50} + 50\left(y_o^- - y^g\right)}\right] \tag{5}$$

$$K^g = \frac{\partial p}{\partial y^g} = \frac{2n\left(p_o^d - C_d p_{ult}\right)}{y_{50} + 2\left|y^g - y_o^g\right|}\left(\frac{y_{50}}{y_{50} + 2\left|y^g - y_o^g\right|}\right)^n + \frac{1.8p_{ult}\dfrac{y_{50}}{50}}{\left(\dfrac{y_{50}}{50} - y^g + y_o^+\right)^2} - \frac{1.8p_{ult}\dfrac{y_{50}}{50}}{\left(\dfrac{y_{50}}{50} - y^g + y_o^-\right)^2} \tag{6}$$

Combined Material

Example behavior for the combined material is shown in Fig. 1 for the second cycle of sinusoidal displacement-controlled loading with amplitude equal to $10y_{50}$. Values of C_d = 0.1, 1.0, and 10.0 are shown in the figure and radiation damping is zero for all cases. The material with C_d=0.1 is pinched in the middle, clearly exhibiting behavior that is consistent with a pile moving through an open gap (e.g., Matlock 1970). Resistance in the open gap arises from friction along the sides of the pile. The force amplitude abruptly increases when the gap closes. The material with C_d=10.0 essentially removes the gap component from the material by making it rigid (notice the essentially rigid response in Fig. 1e).

The tangent modulus for the combined material, K, is defined as $K = (1/K^e + 1/K^p + 1/K^g)^{-1}$. The consistent tangent operator is equal to the elasto-plastic tangent modulus for one dimensional problems, and is important to preserve the quadratic rate of asymptotic convergence for iteration schemes commonly used in nonlinear finite element problems (e.g., Simo and Hughes 1998).

PyLiq1 Material

The PyLiq1 material follows the same logic as the PySimple1 material with the only difference being that the capacity of the p-y material, p_{ult_liq}, is treated as a variable that depends on the mean effective stress in the free-field, σ', rather than being specified as a material constant. The value of p_{ult_liq} is degraded as pore pressure develops in the free field, eventually reaching a residual value p_{res} when σ'=0 according to Eq. 7, where σ_o' is the initial free-field effective stress.

$$p_{ult\_liq} = p_{res} + (p_{ult} - p_{res})\frac{\sigma'}{\sigma_o'} \tag{7}$$

This formulation is intended to incorporate the influence of ground shaking and liquefaction on p-y behavior, while retaining some small p-y capacity for the fully-liquefied condition that has been

observed in many model studies (e.g., Wilson et al. 2000, Dobry et al. 2003). The ground motion and mean effective stress are input to the free-ends of the PyLiq1 elements as demonstrated in Fig. 2. These quantities can be obtained from an effective stress site response analysis, though measured quantities are also used as inputs in this paper. The site response simulation can be run separately from the structural analysis, with the recorded outputs written to file and subsequently input to the free-ends of the p-y elements, or it can be run concurrently with the p-y elements and pile part of the same domain as the soil mesh. If run concurrently, the out-of-plane thickness of the soil mesh should be made very large so that an essentially free-field site response condition is achieved (i.e., so that the pile and p-y elements do not affect the site response). The motivation for utilizing free-field motions is that the p-y materials are intended to capture all of the soil-structure-interaction effects, and none of it is modeled by a soil continuum. A three-dimensional continuum with appropriately sized elements near the pile would be required to properly model SSI effects, and such approaches are computationally very expensive for dynamic problems with liquefaction.

In addition to modeling degradation of the p-y behavior as excess pore pressure develops in the free-field, the material is also capable of modeling the transient stiffening associated with the cyclic mobility behavior of sands in cyclic undrained loading. Cyclic mobility behavior is defined as the transition from incrementally contractive to incrementally dilative behavior that is associated with an increase in the tangent stiffness and inverted s-shaped stress-strain behavior. Cyclic mobility behavior significantly influences free-field site response behavior, and this influence is captured as an input to the PyLiq1 material. However, a limitation of the model is that the dilatancy induced by local strains imposed on the soil by the pile can only indirectly be incorporated by specifying an appropriate value for p_{res}. The concave-upward p-y behavior that has been observed in the absence of shaking-induced free-field dilatancy during blast-induced liquefaction studies (Rollins et al. 2005) and in numerical simulations

(e.g., Iai 2002) is not captured by the PyLiq1 formulation. Furthermore, the inverted cone-shaped negative pore pressure region around the pile that was observed by Gonzalez et al. (2009) is not captured by the PyLiq1 material. Assimaki and Varun (2009) formulated a p-y macroelement that links a Bouc-Wen type backbone curve with a pore pressure function that combines free-field pore pressure response with near-field response related to plastic work in the p-y element. This added feature of material behavior requires specification of additional input parameters for the macro-elements. Development of multiple independent models is important for quantifying the effects of epistemic uncertainty.

An illustration of the PyLiq1 material behavior in level ground conditions (i.e., without static shear stress and lateral spreading) is shown in Fig. 3 for a case where a PyLiq1 material with $p_{res}=0.1p_{ult}$ attaches a soil element to a rigid pile. The soil element is modeled as a PressureDependMultiYield02 material using the default input parameters suggested by Yang et al. (2003) for medium dense sand with D_R =50% , and it is subjected to simple shear loading with a cyclic stress ratio of CSR=0.3. The harmonic simple shear stress path is applied at a low enough frequency to render essentially zero inertial stresses. The simulation was performed in OpenSees, with the soil response computed first and the displacements and mean effective stresses from the soil response subsequently imposed on the free end of the p-y element in a separate analysis. This approach ensures that the soil behavior is a free-field input. The excess pore pressure builds up and reaches 1.0 after approximately 6 cycles, and the material behavior is characterized by transient reductions in pore pressure associated with dilatancy. The dilatant tendency at large strains causes sharp increases in the shear stress when the shear strain exceeds the maximum past strain, resulting in the inverted s-shaped stress-strain behavior that characterizes undrained loading of sands. The p-y behavior in the model mimics the stress-strain behavior of the sand

159 in this case and also exhibits an inverted s-shape that is similar to trends observed in centrifuge tests
160 (e.g., Wilson et al. 2000).

161 An illustration of the PyLiq1 material behavior in the presence of lateral spreading is shown in Fig. 4
162 for the same configuration as in Fig. 3, but with a static shear stress imposed on the soil in addition to
163 the cyclic shear stress. Shear strains accumulate in the direction of static shear stress, resulting in
164 permanent deformation of the soil element in a manner that is consistent with lateral spreading. The
165 free-field soil response was input to the same PyLiq1 material as in Fig. 3, , but this time the analysis was
166 performed for both a rigid pile and for a flexible pile whose stiffness was adjusted so that the peak pile
167 displacement is equal to $10y_{50}$. The rigid pile attracted large loads during each cycle as the soil spreads
168 past, whereas the flexible pile attracted much smaller loads. The flexible pile deformation is
169 characterized by alternating episodes in which (1) the down-slope movement of the sand is slowed as
170 the sand becomes incrementally dilative, the excess pore pressures reduce, and the sand stiffens, (2) the
171 temporarily stiffened sand exerts greater loads on the pile and displaces it down-slope, (3) the dynamic
172 shear stress on the sand reverses direction, such that the sand becomes incrementally contractive, the
173 excess pore pressures increase again, and the sand softens, and (4) the temporarily softened sand exerts
174 lesser loads on the pile, which allows the pile to rebound in the upslope direction. On the other hand,
175 the rigid pile does not displace downslope during dilatancy cycles, and a much larger load is transmitted
176 to the pile due to the cyclic mobility behavior of the soil. This observation is consistent with centrifuge
177 testing by Haigh (2002) that showed that stiff piles attract much larger lateral spreading loads than
178 flexible piles.

179 In addition to PySimple1 and PyLiq1 for lateral soil-pile interaction, TzSimple1 and TzLiq1 materials
180 were formulated for axial shaft friction, and QzSimple1 was formulated for end bearing resistance.
181 TzSimple1 follows the same logic as PySimple1, except the gapping component is removed, and TzLiq1

follows the same logic as PyLiq1, except the residual capacity of the material is set to zero. The backbone of the TzSimple1 and TzLiq1 materials can be selected to match the relation by Mosher (1984) for axially loaded piles in sand, or by Reese and O'Neill (1987) for drilled shafts. QzSimple1 exhibits a direction-dependent response in which a small uplift capacity can be included to model suction stresses in undrained loading. The backbone of the QzSimple1 material can be selected to match the relation by Reese and O'Neill (1987) for drilled shafts in clay or Vijayvergia (1977) for piles in sand. Including axial interaction can be important for pile groups that rotate in response to lateral loading.

Description of Centrifuge Models

Simulations incorporating the PyLiq1 material are compared with experimental data from centrifuge model CSP2 (Wilson et al. 1997) for single piles in nearly level liquefiable sand, and from model SJB03 (Brandenberg et al. 2005) for pile groups in laterally spreading ground. Model sketches are shown in Fig. 5. Properties of the sand utilized in the studies are summarized in Table 1 for CSP2 and Table 2 for SJB03. Peak friction angles reported in Tables 1 and 2 are estimated based on relative density. Pile properties are summarized in Table 3. Results are presented in prototype units unless otherwise specifically noted.

Model CSP2 consisted of a 0.67m diameter single extended pile shaft embedded 16.8m into a horizontally-layered soil profile consisting of liquefiable loose Nevada sand (D_R=35%) over dense Nevada sand (D_R=75%). Pile groups were also embedded in the model, but only the single pile is studied herein. The single pile was at least 15 diameters from the nearest pile group. A 49 MN mass was attached to the top of the pile at a height of 3.81m above the ground surface. The model was saturated with a pore fluid consisting of water mixed with methylcellulose with a viscosity equal to ten times that of water. Testing

was performed at a centrifugal acceleration of 30*g*. Scaling effects related to pore fluid viscosity are discussed by Wilson et al. (2000).

Model SJB03 consisted of a six-pile group of 1.17m diameter piles embedded into a sloping soil profile consisting of a nonliquefiable overconsolidated crust of San Francisco bay mud over loose Nevada sand (D_R=35%) over dense Nevada sand (D_R=75%). A thin layer of Monterey sand was placed on top of the bay mud to prevent desiccation due to wind currents during spinning. The piles were tied together by an embedded pile cap with length x width x height of 14.2m x 9.2m x 2.2m and mass of 726Mg. A channel was carved in the downslope end of the model to simulate a common geologic condition that results in lateral spreading. The model was saturated with water rather than a viscous pore fluid because some water was squeezed out of the clay into the sand during consolidation on the hydraulic press prior to shaking and this water could not be replaced by viscous pore fluid during saturation. Since the viscosity of the pore fluid was not scaled, the prototype hydraulic conductivity of the sand was 57.2 times higher than for the same water-saturated sand at 1-*g*. The hydraulic conductivity is nevertheless low enough to fully liquefy the sand during shaking. Testing was performed at a centrifugal acceleration of 57.2g.

A sequence of ground motions was imposed on each model, and seven of the ground motions imposed on CSP2 and four of the ground motions imposed on SJB03 are analyzed in this paper. The analyzed motions were scaled versions of the UCSC/Lick Lab, Ch. 1 - 90° strong motion record from the 1989 Loma Prieta earthquake, and the downhole record (depth = 83m) from Port Island during the 1995 Kobe earthquake. The ground motion profile was recorded at discrete points using vertical arrays of horizontal accelerometers, and the acceleration records were double-integrated in time to obtain free-field displacement records. The free-field pore pressure profile was recorded using vertical arrays of piezometers. Test CSP2 consisted of a level ground profile and the permanent component of the soil

displacement was negligible, hence time series of ground displacement could be obtained from double integration of acceleration records. On the other hand, the low frequency component of lateral spreading displacement from SJB03 could not be obtained by integration of acceleration records, but was measured using displacement sensors attached to the nonliquefied crust. The complete ground motion time series, including low frequency and high frequency components of the crust displacement, were computed using compatible complementary filters applied to the accelerometer and displacement sensor records. The low frequency components of the soil displacements below the ground surface were assumed to be proportional to those at the ground surface, and the final displaced shape of the soil profile (as determined from post-test profiles of vertical markers embedded in the model) was used to determine the coefficients of proportionality for those low frequency components. Displacement time series were then computed by combining the low and high frequency components. Validation of this procedure and the selection of appropriate filters for the equipment used in these centrifuge tests are discussed in Kutter and Balakrishnan (1998).

Material Properties for p-y, t-z, and Q-z elements

The capacity of the p-y materials, p_{ult}, was estimated using the API (1993) equations for piles in sand. A p-multiplier approach was to define the residual capacity as $p_{res} = m_p p_{ult}$, where m_p was defined based on Brandenberg (2005). The modulus of subgrade reaction in sand deposits is often assumed to vary linearly with depth, however the elastic modulus for clean sands is known to vary approximately with the square root of confining stress (e.g., Yamada et al. 2008). Hence, a parabolic relation was used to define the elastic stiffness with depth. The crust load acting on the embedded pile cap for test SJB03 was estimated to be 6940kN based on the sum of passive earth pressure and side and base friction summarized by Brandenberg et al. (2005). Pile group effects are considered for the mobilized crust load because clay may become trapped between the piles, thereby causing the pile group to act as an

equivalent block (Brandenberg et al. 2005). However, group effects are not included for the sand layers based on tests that show group interaction effects to be negligible in liquefied soils (Rollins et al. 2005). Lateral load transfer between pile groups and nonliquefied crusts was observed to be significantly softer for crusts spreading over liquefied soil compared with nonliquefied soil profiles (Brandenberg et al. 2007a). The p-y materials in the nonliquefied crust were therefore adjusted so that the ultimate capacity was mobilized at a relative displacement of 40% of the crust thickness rather than a more typical value of 1 to 7% of the crust thickness observed in load tests in nonliquefied soil profiles.

The single-pile for CSP2 required only p-y elements to model lateral load transfer, but the pile group in SJB03 required t-z elements to model shaft friction and Q-z elements to model end bearing since the pile group forms a frame that can rock during lateral loading. The t-z elements were modeled using TzLiq1 materials with $t_{ult}=K_oB\sigma_{vo}'\tan(2/3\phi')$, where $K_o = 1-\sin\phi'$, and σ_{vo}' is the initial vertical effective stress prior to shaking. Horizontal stresses at the soil-pile interface typically increase when closed-ended pipe piles are driven into the soil. However, in this case the piles were driven into the models at 1*g*, therefore significant changes in horizontal pressure are not anticipated. The bearing capacity at the tip of the piles was estimated to be 10MN using bearing factors by Meyerhof (1976), and end bearing resistance was modeled using QzSimple1 materials since there was little excess pore pressures generated in the end bearing stratum in each case.

Numerical Modeling Approach

Numerical models of the pile were constructed in OpenSees (McKenna and Fenves 2001) using 50 elements along the length of the pile with p-y elements attached at each node below the ground surface. For CSP2 the piles did not yield during testing, and were therefore modeled as elasticBeamColumn elements with properties summarized in Table 3. A mass was assigned to the top

node. For SJB03, the piles did slightly yield during testing, and were therefore modeled using nonlinear beam column elements. The piles were tied together at their head by a pile cap composed of very stiff (essentially rigid) beam column elements. An elastic rotational element attached the pile head to the pile cap to model the measured rotational stiffness of 1300 MN-m/rad at the connection. Masses were distributed among the pile cap nodes and PyLiq1 materials were attached to the top and bottom of the pile cap. For convenience, PyLiq1 materials were utilized for the nonliquefied crust layer as well as in the liquefiable layers but the recorded mean effective stress time series input to the free-ends of the crust were essentially constant since the clay did not generate significant excess pore pressure during the tests. Hence, the PyLiq1 material response was nearly identical to what the PySimple1 material response would have been. TzLiq1 materials were distributed along the length of the piles and QzSimple1 materials were attached to the pile tips. This configuration permits the pile group to rotate during lateral loading, which is an important feature of the response of laterally loaded pile groups. The free-ends of the t-z and Q-z elements were fixed.

Time series of displacement and mean effective stress were linearly interpolated from the recorded data, and imposed on the free-ends of the p-y elements. Recordings of acceleration and pore pressure were from sensors at least 10 pile diameters from the nearest foundation. In forward predictions, displacements and pore pressures would need to be estimated from a site response simulation. However, in this study the measured inputs are utilized to isolate the response of the PyLiq1 materials so that errors in the p-y elements could be separated from errors in site response simulations. Small-strain damping of approximately 2% in the frequency range of interest was achieved using Rayleigh damping. The convergence tolerance on the norm of the displacement residuals was set to 10^{-6} (using the normDispIncr command), and displacement constraints were enforced using the transformation method (using the Transformation command). The equation of motion was integrated using the Hilbert-

Hughes-Taylor integrator (using the HHT command) with α=0.7. The time step was adjusted as needed to facilitate convergence (using the VariableTransient command).

Numerical Results for CSP2

Example analysis results for CSP2 are shown in Fig. 6 for a Santa Cruz motion with a peak base acceleration of 0.42g. The excess pore pressure ratio near the center of the loose sand layer reaches 1.0 approximately 5s after the start of strong shaking, and subsequently exhibits modest dilation-induced drops in pore pressure. Excess pore pressure ratios are plotted in the free-field, far away from the pile groups, and also at a location immediately adjacent to the pile. Dilation-induced spikes are apparent in both records, but are slightly more pronounced in the record near the pile, presumably due to the additional increment of dilatancy caused by strains imposed on the near field soil by the pile. The peak bending moment (measured and predicted) is mobilized during one such dilation-induced drop in pore pressure at approximately time = 26s. The bending moment and superstructure acceleration records are predicted quite well. The bending moment record was taken at a depth of approximately 3B, where the peak bending moments were measured. Computed values of subgrade reaction near the center of the loose sand do not agree with measurements as well as computed values of bending moment and superstructure acceleration, but nevertheless, the peak responses are predicted well during critical cycles. Furthermore, the "measured" subgrade reaction values were obtained by double-differentiation of recorded bending moments, and are prone to more significant measurement error than the measured bending moment and superstructure acceleration (particularly at high frequencies).

The same records from Fig. 6 are plotted in Fig. 7 for a Kobe motion with a peak base acceleration of 0.61g. The frequency content of the Kobe motion is significantly lower than the Santa Cruz motion, and the dilatancy response in the liquefied sand in much more pronounced as a result. Once again, the peak

316 bending moment and peak superstructure acceleration occurred during a transient drop in excess pore
317 pressure. The superstructure acceleration reached a peak near 1.5g that was under-predicted by the
318 analyses by about 0.5g, but the computed values track the measured response quite well other than for
319 the one cycle that produced the peak value. The bending moment mobilized in the pile is also predicted
320 reasonably well.

321 Acceleration response spectra were computed for the superstructure motion for three Santa Cruz
322 motions and four Kobe motions of various intensities. The shapes of the spectra tend to agree quite well
323 with measurements. However, for the Santa Cruz motions, the computed values tend to be too high for
324 the high-intensity motions and too low for the low-intensity motions. For the Kobe motions, the
325 disagreements could not be so simply characterized based on input motion intensity. Better agreement
326 could be achieved by adjusting the stiffness of the p-y materials on a motion-specific basis by increasing
327 K_{ref} for the small motions and decreasing K_{ref} for the large motions. This may partly reflect the effect of
328 loading history on p-y behavior, which is not included in the analyses. Another factor may be that the
329 functional form of the API (1993) sand curve is very linear at small values of y, hence there is very little
330 small-strain nonlinearity in the PyLiq1 materials. Recent research by Varun (2010) also demonstrated
331 that the API curve is too linear, and suggested an alternative form that resulted in better agreement
332 with measurements.

333 **Numerical Results for SJB03**

334 Computed results for SJB03 are compared with measurements for the medium intensity Santa Cruz
335 motion with peak base acceleration of 0.35g in Fig. 9. Some residual loads were present in the pile
336 groups at the end of each motion for SJB03 due to lateral spreading deformations and the motions were
337 applied in sequence in the numerical simulations, which explains the non-zero initial values of some

quantities in Fig. 9. The excess pore pressure ratio in the loose sand does not reach 1.0 for this motion even though surface evidence of liquefaction was observed in the form of 0.4m of lateral spreading ground displacement. This may be attributed to the effect that sustained downslope shear stresses has on limiting values of excess pore pressure ratio (e.g., Ishihara and Nagase 1980). Computed values are reasonably consistent with the measurements for bending moment, crust load, pile cap inertia, and pile cap displacement, though the residual loads on the pile group are larger than predicted.

Computed values for the large Kobe motion with peak base acceleration of 0.67g are shown in Fig. 10. This motion fully liquefied the loose sand in the first cycle of strong shaking, and the response is characterized by very pronounced dilatancy spikes. Each downward spike in the pore pressure record is associated with a local peak in the crust load, a local minimum bending moment (the largest amplitude bending moments were negative in this case), and a local maximum in pile cap inertia. The crust load sometimes exceeded the predicted maximum crust load, and as a result the peak bending moments were slightly under-predicted in the analysis. Nevertheless, agreement between the measured and predicted responses is quite reasonable.

Response spectra for the pile cap motion are shown in Fig. 11. The shape of the spectra was reasonably predicted in each case, though the amplitude was not predicted perfectly. Once again, the small-strain stiffness of the p-y materials could be adjusted to provide a better prediction of pile cap motion (results not shown for brevity), which may either represent the effects of loading history not being accounted for in the analyses or indicate a need for a p-y material functional form that more correctly captures small-strain nonlinearity.

Discussion

A key feature of the PyLiq1 material is that it incorporates not only the development of excess pore pressure during cyclic loading, but also transient reductions in pore pressure caused by dilatancy. Dilatancy was shown to be an important driver of peak bending moments in the pile foundations from centrifuge studies by Wilson et al. (2000) and Brandenberg et al. (2005). This paper input the measured pore pressure response, hence the dilatancy response was included to the extent it was measured in the free-field during a particular motion. However, the pore pressure response would need to be numerically simulated in a forward analysis. Advanced plasticity models are capable of capturing the dilatancy response (e.g., Dafalias and Manzari 2004; Yang et al. 2003, Boulanger 2010) whereas other models can capture the development of excess pore pressure but not the transient reductions caused by dilatancy (e.g., Martin and Qiu 2001). To explore the influence of dilatancy on pile response, simulations for the single pile from CSP2 were repeated with the same displacement records input to the free-ends of the p-y materials, but with the measured pore pressure response adjusted so that it only increased (Fig. 12). The motions in Fig. 12 were selected because in both cases the loose sand fully liquefied, but the extent of the post-liquefaction dilatancy-induced drops in pore pressure were quite different. The Santa Cruz motion exhibited very small pore pressure drops whereas the Kobe motion exhibited very pronounced drops.

For the Santa Cruz motion, the simulation with the always-increasing pore pressure record is very similar to the simulation that utilized the measured pore pressure input. On the other hand, significant differences arise for the Kobe motion, where the always-increasing pore pressure response resulted in a significantly smaller prediction of peak bending moments and superstructure acceleration (Table 4). These cases demonstrate that dilatancy can be a significant factor that drives the critical loading cycles for piles in liquefied ground. Similarly, Kramer et al. (2011) and Ziotopoulou et al. (2011) illustrate that

dilatancy is an important factor in obtaining reasonable simulations of the seismic responses of liquefying soil profiles.

The cases studied in this paper involved liquefaction of loose sands. Wilson et al. (2000) studied liquefaction potential of medium dense sands and found them to be more dilatant and exhibit more pronounced cyclic mobility behavior compared with the looser sands. Analysis of a medium dense sand case is presented by Boulanger et al. (2004).

Conclusions

Static methods for analyzing piles in liquefied ground are appropriate for many structures for which dynamic simulations are too complex and costly, and uncertainties inherent to static analysis approaches can be accommodated by adequate conservatism. However, dynamic simulations may be warranted for important structures, and may be required for complex structures for which liquefaction-compatible inertia demands are difficult to quantify without performing a dynamic simulation. Advancing beyond equivalent static analysis of piles in liquefied ground requires development of robust, validated numerical tools for performing dynamic simulations. This paper addresses this need by formulating liquefiable soil-structure interaction elements that utilize free-field site response quantities as inputs.

Comparisons with centrifuge test data show that the materials can reasonably capture key features of dynamic response when measured displacements and excess pore pressures are utilized as inputs. Forward predictions would require a site response simulation to obtain ground motion and effective stress time series to input to the p-y model, which introduces additional uncertainty to the predictions. The measured inputs were utilized instead of a site response prediction in this study to isolate the behavior of the p-y materials.

Cyclic mobility behavior that is associated with inverted s-shaped stress strain behavior during undrained loading of sands also causes inverted s-shaped p-y behavior for piles embedded in liquefied sand. Cyclic mobility behavior was found to be the mechanism responsible for mobilization of the peak bending moments in the piles presented in this study. Simulations that neglected cyclic mobility behavior (i.e., by inputting an always-increasing pore pressure response) under-predicted bending moments and superstructure accelerations compared with measurements, and compared with simulations that included cyclic mobility behavior. Therefore, neglecting the influence of cyclic mobility on pile response could result in unconservative predictions and unforeseen damage or failure.

Acknowledgments

Funding for this work was provided by Caltrans and the National Science Foundation through the Pacific Earthquake Engineering Research Center. The contents of this paper do not necessarily represent a policy of either funding agency or endorsement by the state or federal government. The authors would like to thank Christina Curras for doing the initial model development work on the p-y material models prior to their implementation in OpenSees. Tom Shantz provided valuable technical guidance. The centrifuge shaker was designed and constructed with support from the National Science Foundation (NSF), Obayashi Corp., Caltrans, and the University of California. Upgrades were funded by NSF award CMS-0086566 through the George E. Brown, Jr. Network for Earthquake Engineering Simulation (NEES).

Notation

B = pile diameter

C = modeling constant that contributes to shape of p-y backbone curve

C_r = modeling constant that controls size of elastic region

C_d = modeling constant that controls subgrade reaction load in open gap

CSR = cyclic stress ratio

D_R = relative density

K_o = coefficient of at-rest earth pressure

K = tangent stiffness of p-y element

K^e = tangent stiffness of elastic component

K^p = tangent stiffness of plastic component

K^g = tangent stiffness of gap component

n = modeling constant that contributes to shape of p-y backbone curve

p = subgrade reaction due to relative displacement between soil and pile

p^d = component of subgrade reaction in drag element

p^c = component of subgrade reaction in closure element

p_α = subgrade reaction value at center of elastic region

p_{res} = ultimate resistance of p-y element for fully-liquefied condition (i.e., with r_u=1)

p_{ult} = ultimate resistance of p-y element for non-liquefied condition (i.e., with r_u=0)

p_{ult_liq} = ultimate resistance of p-y element corresponding to $0 < r_u < 1$

p_o = value of subgrade reaction at start of current plastic loading cycle

p_o^d = component of subgrade reaction in drag element at start of current plastic loading cycle

r_u = excess pore pressure ratio

t_{ult} = ultimate shaft friction load per unit pile length

y = relative displacement between soil and pile

y_{50} = relative displacement between soil and pile when half of ultimate load is mobilized in p-y element

y^e = elastic component of relative displacement between soil and pile

y^p = plastic component of relative displacement between soil and pile

y^g = gap component of displacement between soil and pile

y_o^g=value of gap component of relative displacement between soil and pile at start of current plastic loading cycle

451 y_o^p = value of plastic component of relative displacement between soil and pile at start of current plastic
452 loading cycle

453 y_o^+ = gap evolution term equal to maximum past value of y^e+1.5y_{50}

454 y_o^- = gap evolution term equal to maximum past value of y^e-1.5y_{50}

455 ϕ' = peak friction angle

456 σ' = current effective stress in free-field soil

457 σ_o' = initial effective stress in free-field soil

458 σ_{vo}' = vertical effective stress

459

460 **References**

461 Abdoun, T., Dobry, R., O'Rourke, T. D., and Goh, S. H. (2003). ''Pile response to lateral spreads:
462 Centrifuge modeling.'' *J. Geotech. Geoenviron. Eng., ASCE.* 129(10), 869–878.

463 American Petroleum Institute (API). (1993). *Recommended Practice for Planning, Design, and*
464 *Constructing Fixed Offshore Platforms*. API RP 2A - WSD, 20th ed., American Petroleum Institute.

465 Ashford S.A., Rollins, K.M., and Lane, D. (2004). "Blast-Induced Liquefaction for Full-Scale Foundation
466 Testing," Journal of Geotechnical and Geoenvironmental Engineering,ASCE, 130(8), pp. 798-806.

467 Assimaki, D., and Varun. (2009). "Nonlinear Macroelements for Performance-Based Design of Pile-
468 Supported Waterfront Structures in Liquefiable Sites," *Proceedings, International Conference on*
469 *Performance-Based Design in Earthquake Geotechnical Engineering*, Paper No. 253, pp. 1791-1798.
470 T. Kokusho et al., Eds. London: Taylor and Francis Group.

471 Boulanger, R.W. (2010). "A sand plasticity model for earthquake engineering applications." University of
472 California, Davis. Report No. UCD/CGM-10/01. 77p.

473 Boulanger, R. W., Chang, D., Brandenberg, S. J., Armstrong, R. J., and Kutter, B. L. (2007). "Seismic design
474 of pile foundations for liquefaction effects." Earthquake Geotechnical Engineering, 4th International

475 Conference on Earthquake Geotechnical Engineering – Invited Lectures, K. D. Pitilakis, ed., Springer,
476 The Netherlands, 277-302.
477 Brandenberg, S.J., Boulanger, R.W., Kutter, B.L., and Chang, D. (2005). "Behavior of pile foundations in
478 laterally spreading ground during centrifuge tests." *J. Geotech. Geoenviron. Eng.*, ASCE., 131(11),
479 1378-1391.
480 Brandenberg, S.J., Boulanger, R.W., Kutter, B.L., and Chang, D. (2007a). "Liquefaction-induced softening
481 of load transfer between pile groups and laterally spreading crusts." J. Geotech. Geoenviron. Eng.,
482 ASCE, 133(1). 91-103.
483 Brandenberg, S.J., Boulanger, R.W., Kutter, B.L., and Chang, D. (2007b). “Static pushover analyses of pile
484 groups in liquefied and laterally spreading ground in centrifuge tests.” J. Geotech. Geoenviron. Eng.,
485 ASCE, 133(9), 1055-1066.
486 Dafalias, Y.F., and Manzari, M.T. (2004). "Simple plasticity sand model accounting for fabric change
487 effects." *J. Eng. Mech.* 130(6). 622-364.
488 Dobry, R., Abdoun, T., O’Rourke, T. D., and Goh, S. H. (2003). "Single Piles in Lateral Spreads: Field
489 Bending Moment Evaluation." *J. Geotech. Geoenviron. Eng.,* ASCE, Vol. 129(10), 879-889.
490 González, L., Abdoun, T., and Dobry, R. (2009). "Effect of soil permeability on centrifuge modeling of pile
491 response to lateral spreading." *J. Geotech. Geoenviron. Eng.*, ASCE, 135(1), 62-73.
492 Haigh, S. K. (2002). "Effects of earthquake-induced liquefaction on pile foundations in sloping ground."
493 Ph.D. dissertation, Cambridge University, UK.
494 Haigh, S.K. & Madabhushi, S.P.G. (2011) Centrifuge modeling of pile-soil interaction in liquefiable slopes.
495 Geomechanics and Engineering **3**(1) 1-16
496 Iai, S. (2002). "Analysis of soil deformation around a cylindrical rigid body." Proc. U.S.-Japan Seminar on
497 Seismic Disaster Mitigation in Urban Area by Geotechnical Engineering, I. Towhata and R. W.
498 Boulanger, eds., Anchorage, Alaska, June.

Ishihara, K., and Nagase, H. (1980). "Cyclic simple shear tests on saturated sand in multi-directional loading," by Ishihara and Yamazaki (1980). Soils and Foundations, Japanese Society of Soil Mechanics and Foundation Engineering, 20(1), March. Closure to discussion.

Juirnarongrit, T., and Ashford, S.A. (2006). “Soil-Pile Response to Blast-Induced Lateral Spreading. II: Analysis and Assessment of the p-y Method,” Journal of Geotechnical and Geoenvironmental Engineering, ASCE, 132(2), pp. 163-172.

Kramer, S. L., A. J. Hartvigsen, S. S. Sideras, and P. T. Ozener (2011), "Site Response Modeling in Liquefiable Soil Deposits", 4th IASPEI / IAEE Intl. Symposium, Effects of Surface Geology on Seismic Motion, Univ. of California, Santa Barbara, August 23-26.

Kutter, B.L., and Balakrishnan, A. (1998) “Dynamic model test data from electronics to knowledge,” *Proc. Centrifuge ’98*, T. Kimura, O. Kusakabe, and J. Takemura, eds., pp. 931–943, A. A. Balkema Publishers, (Rotterdam, Netherlands).

Matlock, H. (1970). "Correlations of design of laterally loaded piles in soft clay." *Proc. Offshore Technology Conference*, Houston, TX, Vol 1, No.1204, pp. 577-594.

Matlock, H., Foo, S. H., and Bryant, L. L. (1978). ‘‘Simulation of lateral pile behavior.’’ *Proc., Earthquake Engrg. and Soil Dyn.*, ASCE, New York, 600–619.

McKenna, F., and Fenves, G.L. (2001). "OpenSees Manual." PEER Center, http://OpenSees.berkeley.edu.

Martin, G.R., and Qiu, P. (2001), “Site Liquefaction Evaluation: The Application of Effective Stress Site Response Analyses,” draft technical report prepared for the Multidisciplinary Center for Earthquake Engineering Research, Buffalo, NY.

Mosher, R.L. (1984). "Load Transfer Criteria for Numerical Analysis of Axial Loaded Piles in Sand." US Army Engineering Waterways Experimental Station, Automatic Data Processing Center, Vicksburg, Mississippi, January.

522 Reese, L. C. and M. W. O'Neill. (1987). "Drilled Shafts: Construction Procedures and Design Methods."
523 Report No. FHWA-HI-88-042, U.S. Department of Transportation, Federal Highway Administration,
524 Office of Implementation, McLean, Virginia.
525 Reese, L. C., Wang, S. T., Isenhower, W. M., Arrelaga, J.A., and Hendrix, J. A. (2000). *LPILE Plus Verion*
526 *4.0m,* Ensoft, Inc. Austin, TX.
527 Rollins, K.M., Gerber, T.M., Lane, J.D. and Ashford. S.A. (2005). "Lateral Resistance of a Full-Scale Pile
528 Group in Liquefied Sand." J. Geotechnical and Geoenvironmental Engrg., ASCE, Vol. 131, No. 1, p.
529 115-125.
530 Simo, J.C., and Hughes T.J.R. (1998). Computational Inelasticity. Springer, New York. 392 p.
531 Tokimatsu, K. and Suzuki, H. (2004). "Pore water pressure response around pile and its effects on p-y
532 behavior during soil liquefaction." Soils and Foundations, 44(6), 101-110.
533 Vijayvergiya, V. N. (1977). "Load-Movement Characteristics of Piles." Proceedings, Ports 77 Conference,
534 American Society of Civil Engineers, Long Beach, California, March.
535 Wilson, D.W., Boulanger, R.W., and Kutter, B.L. (1997). "Soil-pile-superstructure interaction at soft or
536 liquefiable soils sites - centrifuge data report for CSP2." UCD/CGMDR-97/03. University of California,
537 Davis.
538 Wilson, D. W., Boulanger, R. W., and Kutter, B. L. (2000). "Seismic lateral resistance of liquefying sand." *J.*
539 *Geotech. Geoenviron. Eng.*, ASCE, 126(10): 898-906.
540 Yamada, S., Hyodo, M., Orense, R.P., Dinesh, S.V., and Hyodo, T. (2008). "Strain-dependent dynamic
541 properties of remolded sand-clay mixtures." *J. Geotech. Geoenviron. Eng.*, 134(7), 972-981.
542 Yang, Z., Elgamal, A., and Parra, E., (2003). "A Computational Model for Liquefaction and Associated
543 Shear Deformation," *Journal of Geotechnical and Geoenvironmental Engineering*, ASCE, Vol. 129, No.
544 12.

545 Ziotopoulou, K., Boulanger, R. W., and Kramer, S. L. (2012). "Site response analysis of liquefying sites."
546 Proceedings, Geocongress 2012, ASCE, Oakland, CA.

Figure 1. Example p-y behavior for PySimple1 material showing (a) the element configurations, (b) to (e) the contributions of each component, and (f) the overall material response.

Figure 2. Schematic showing ground motion and mean effective stress from site response analysis input to free ends of PyLiq1 elements.

Figure 3. Response of PressureDependMultiYield02 material to cyclic simple shear stress path, and of PyLiq1 material attaching soil element to a rigid pile.

Figure 4. Response of PressureDependMultiYield02 material to cyclic simple shear loading and static shear stress, and PyLiq1 material attached to rigid pile and flexible pile.

Figure 5. Model sketches for centrifuge tests (a) CSP2 and (b) SJB03.

Figure 6. Measured and predicted time series for single pile from test CSP2, Santa Cruz motion "j".

Figure 7. Measured and predicted time series for single pile from test CSP2, Kobe motion "l".

Figure 8. Acceleration response spectra (5% damping) for measured and predicted superstructure motion for test CSP2 for (a) three Santa Cruz motions, and (b) four Kobe motions, of varying intensity.

Figure 9. Measured and recorded time series from test SJB03 for the medium intensity Santa Cruz motion.

Figure 10. Measured and predicted time series from test SJB03 for the large intensity Kobe motion.

Figure 11. Acceleration response spectra (5% damping) for measured and predicted pile cap motion for (a) three Santa Cruz motions of varying intensity, and (b) one Kobe motion.

Figure 12. Influence of dilatancy on pile response is small for (a) Santa Cruz motion and large for (b) Kobe motion.

Table
Click here to download Table: Tables.doc

Table 1. Soil properties for centrifuge model CSP2.

Soil Layer	Depth to Top of Layer (m)	γ (kN/m^3)	D_R (%)	ϕ'_{pk} (deg)	V_s (m/s)[a]	K_{ref} (kN/m^3)[b]	m_p[c]
Loose Nevada Sand	0	19	35	32°	170	12500	0.05
Dense Nevada Sand	9.1	20	75	38°	230	55500	0.3

[a] Shear wave velocity based on measurements from SJB03 for sand with same relative density.

[b] Modulus of subgrade reaction, $K = K_{ref}(\sigma_v'/50kPa)^{0.5}$.

[c] p-multipliers based on Brandenberg (2005).

Table 2. Soil properties for centrifuge model SJB03.

Soil Layer	Depth to Top of Layer (m)	γ (kN/m^3)	D_R (%)	ϕ'_{pk} (deg)	s_u (kPa)[a]	V_s (m/s)[b]	K_{ref} (kN/m^3)[c]	m_p[d]
Monterey Sand	0	17	--	36°	--	--	--	--
Bay Mud	1.2	16	--	--	44	160	--	--
Loose Nevada Sand	3.9	19	35	32°	--	170	12500	0.05
Dense Nevada Sand	9.4	20	75	38°	--	230	55500	0.3

[a] Average value for thickness of clay layer measured using T-bar.

[b] Shear wave velocity measured in-flight using mini air hammers.

[c] Modulus of subgrade reaction, $K = K_{ref}(\sigma_v'/50kPa)^{0.5}$.

[d] p-multipliers based on Brandenberg (2005).

Table 3. Pile properties.

Test	b (m)	E (GPa)	I (m^4)	A (m^4)	M_y (kPa)[a]
CSP02	0.67	68.9	6.06×10^{-3}	0.135	7522
SJB03	1.17	68.9	22.0×10^{-3}	0.166	17050

Table 4. Peak superstructure acceleration and pile bending moment predicted with and without dilatancy effects compared with measured quantities. Percent error is indicated in parenthesis.

	Santa Cruz			Kobe		
	Measured	PyLiq1	No Dilatancy	Measured	PyLiq1	No Dilatancy
Superstructure acceleration (g)	0.24	0.35 (+46%)	0.37 (+54%)	1.54	1.25 (-18%)	0.78 (-97%)
Pile bending moment (kN·m)	490	896 (+83%)	971 (+98%)	3464	3189 (-9%)	2144 (-38%)

Figure1
Click here to download high resolution image

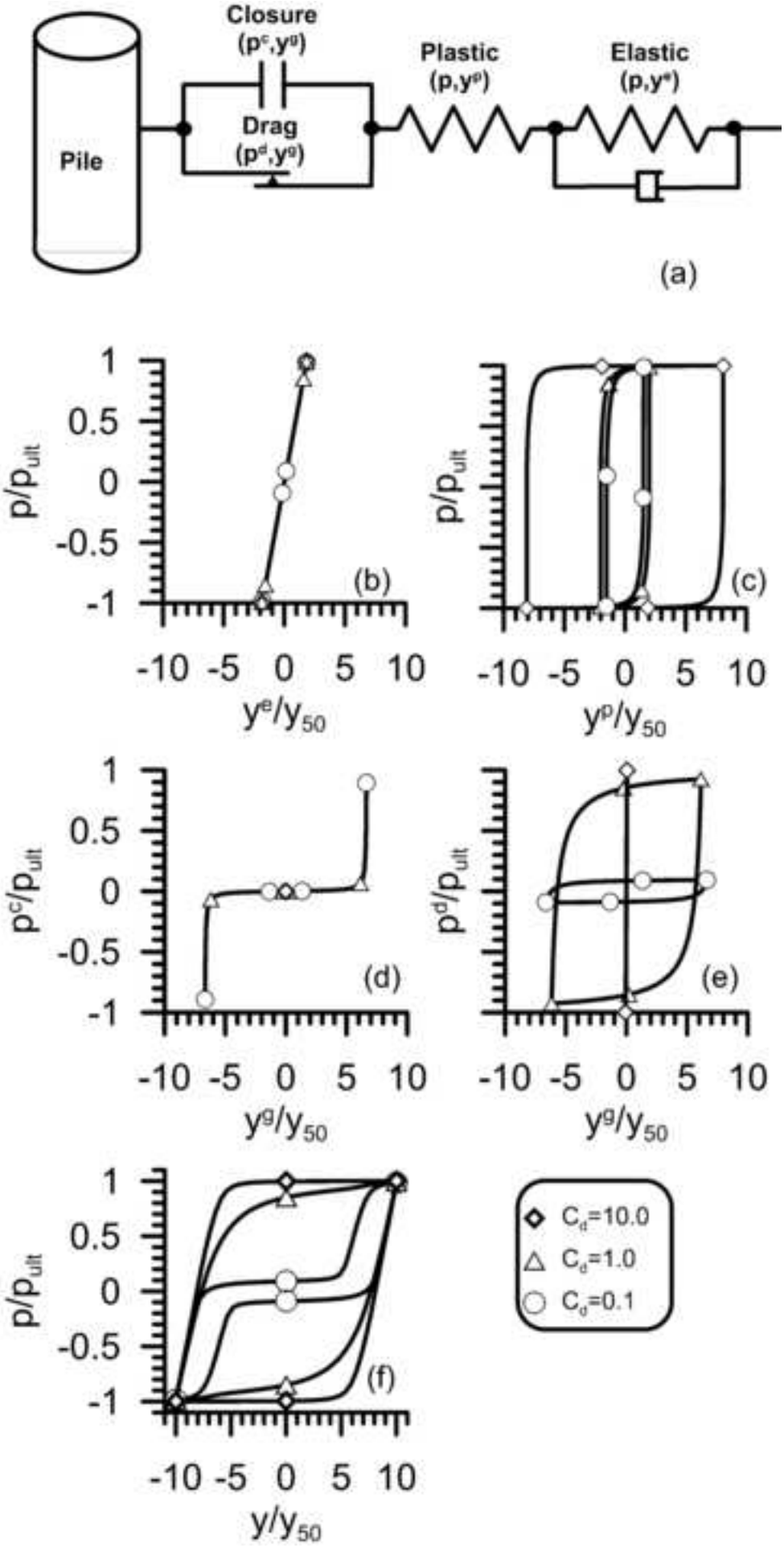

Figure2
Click here to download high resolution image

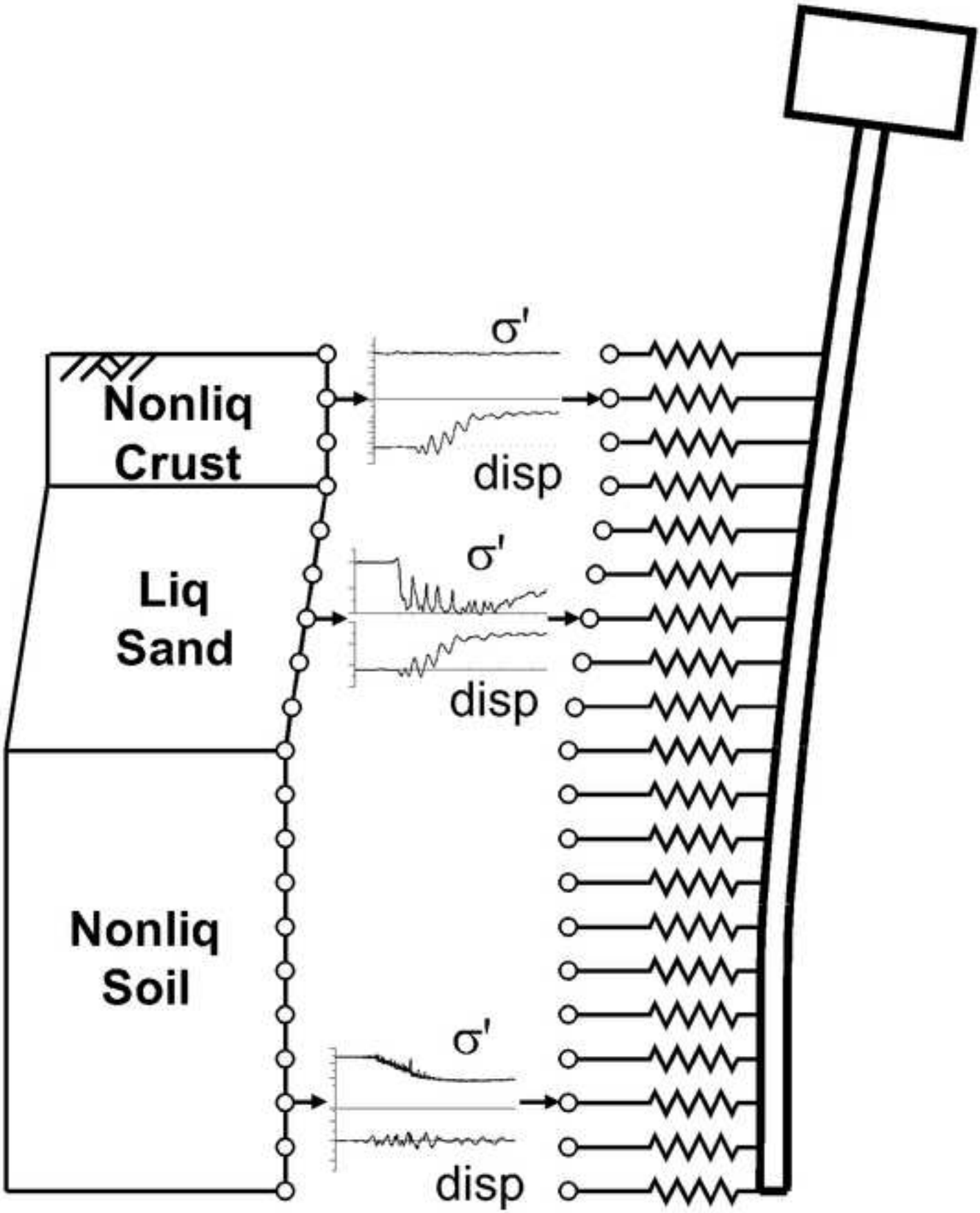

Figure3
Click here to download high resolution image

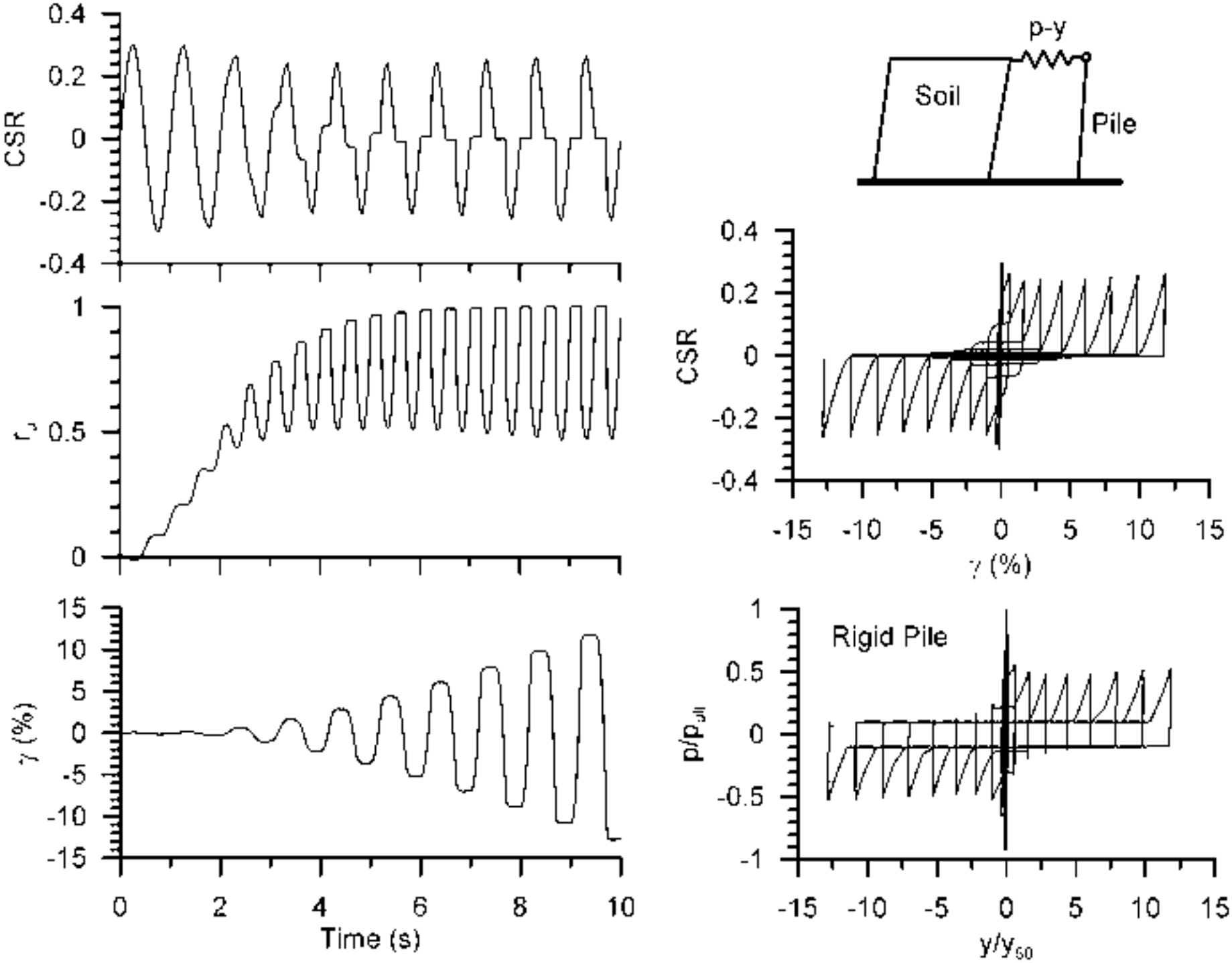

Figure4
Click here to download high resolution image

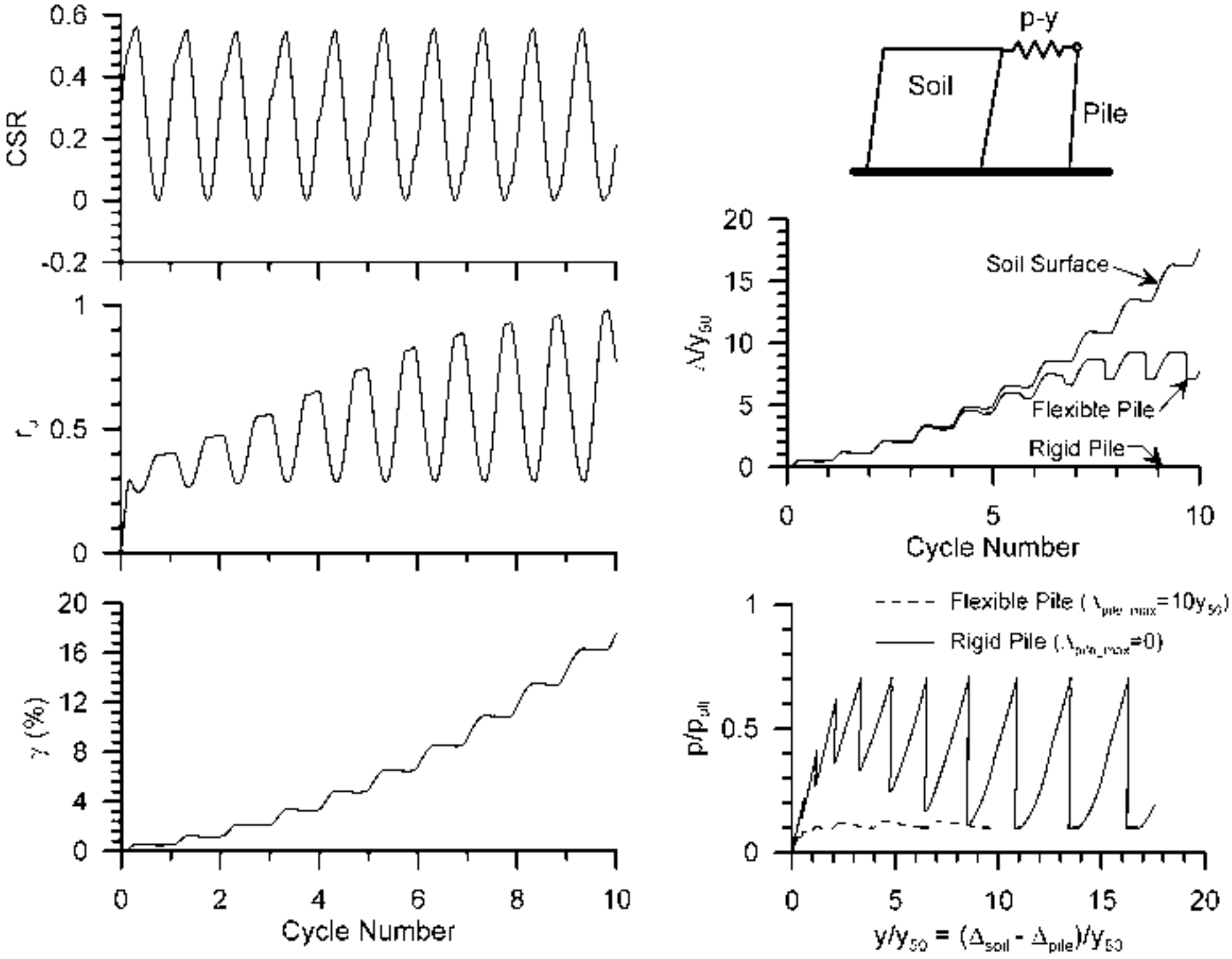

Figure5
Click here to download high resolution image

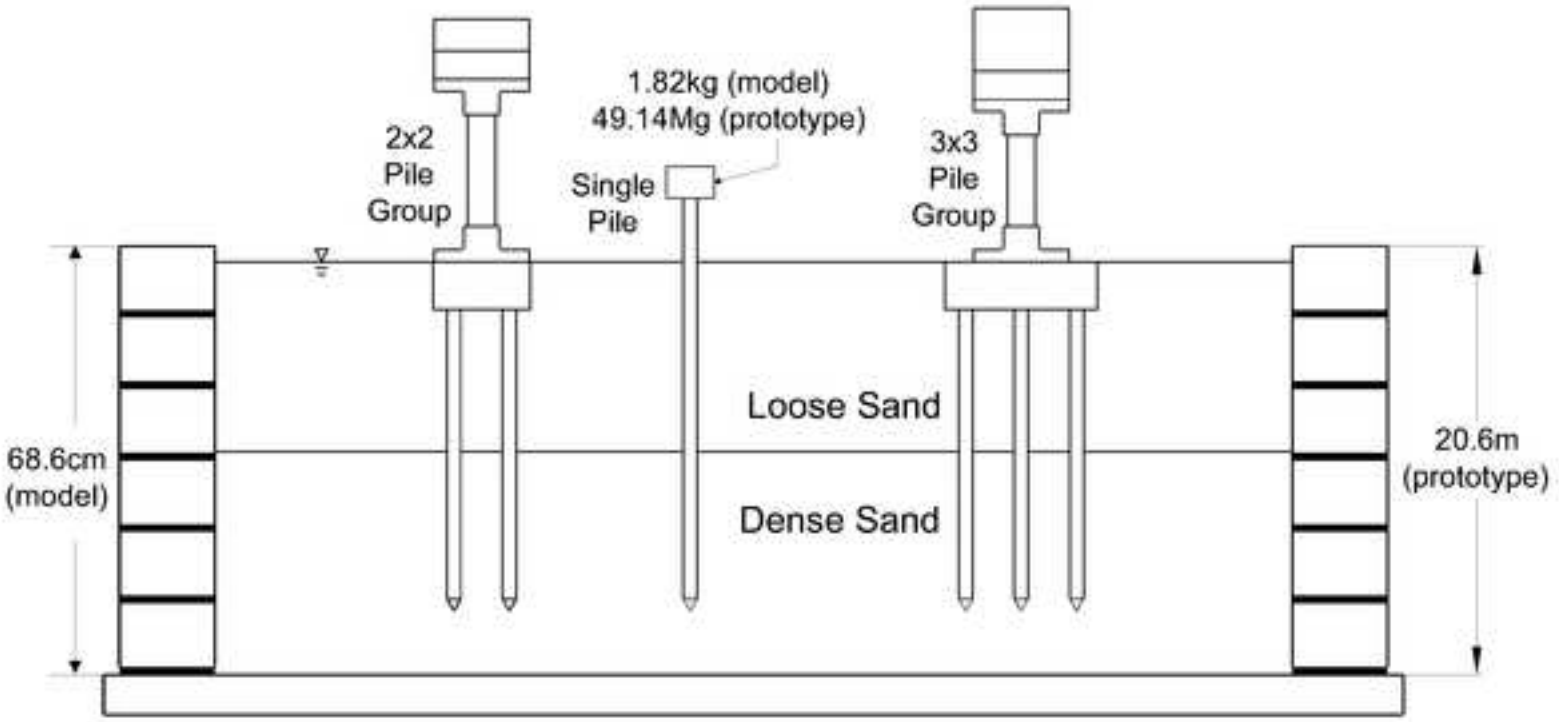

(a) CSP2

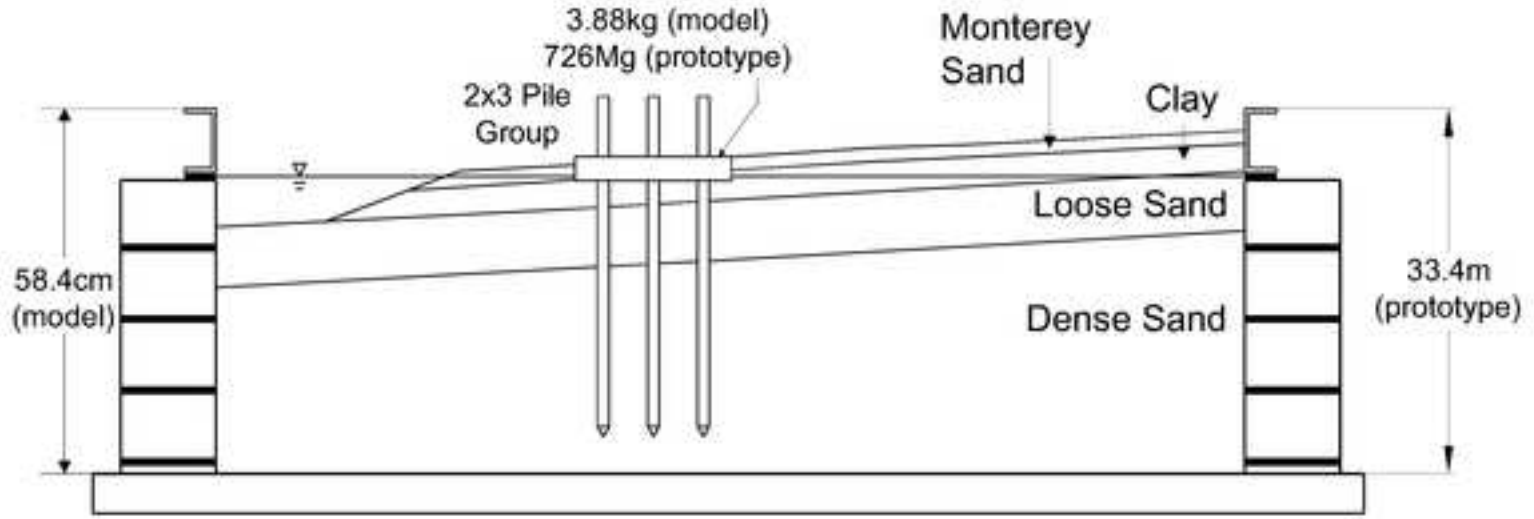

(b) SJB03

Figure6
Click here to download high resolution image

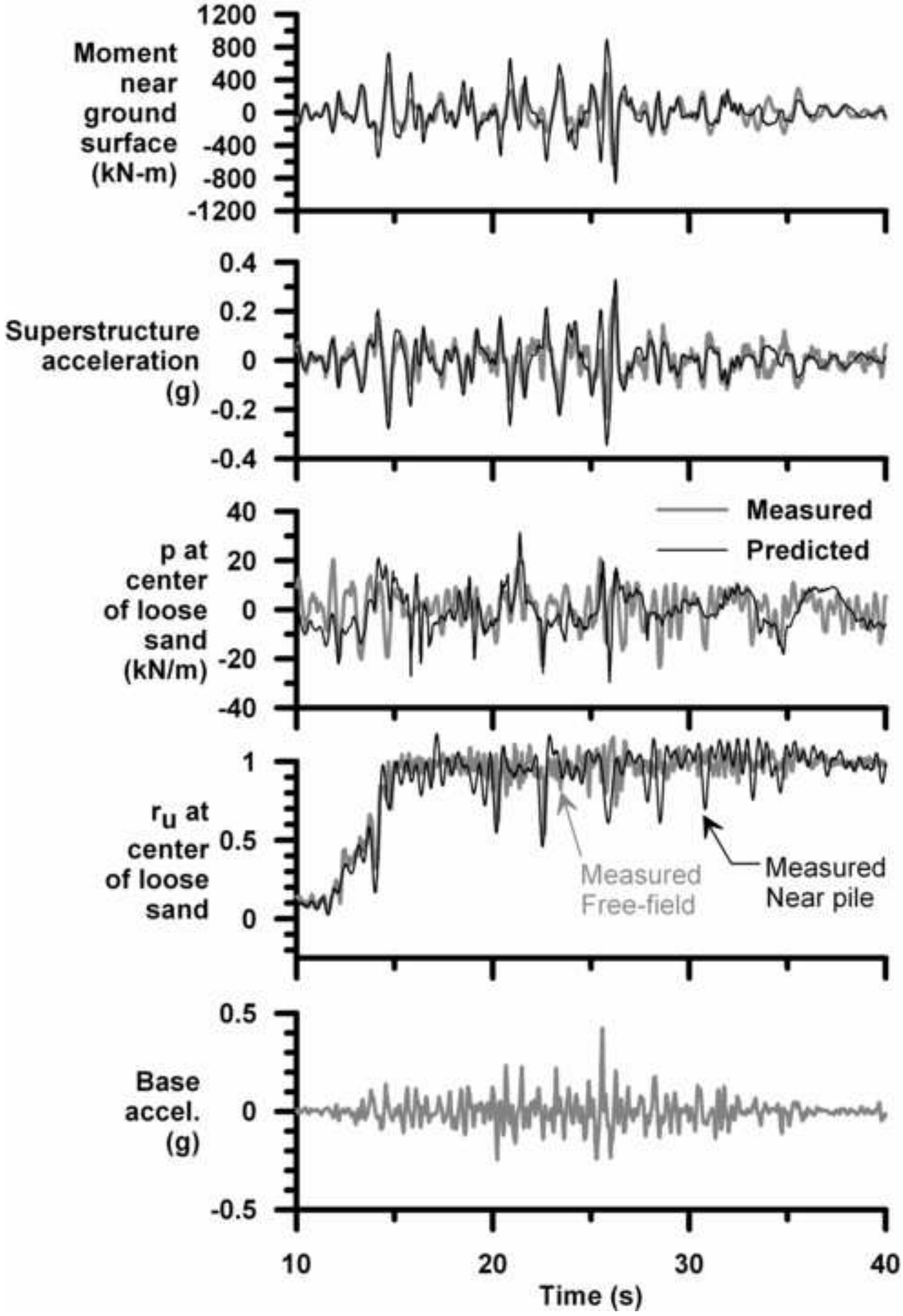

Figure7
Click here to download high resolution image

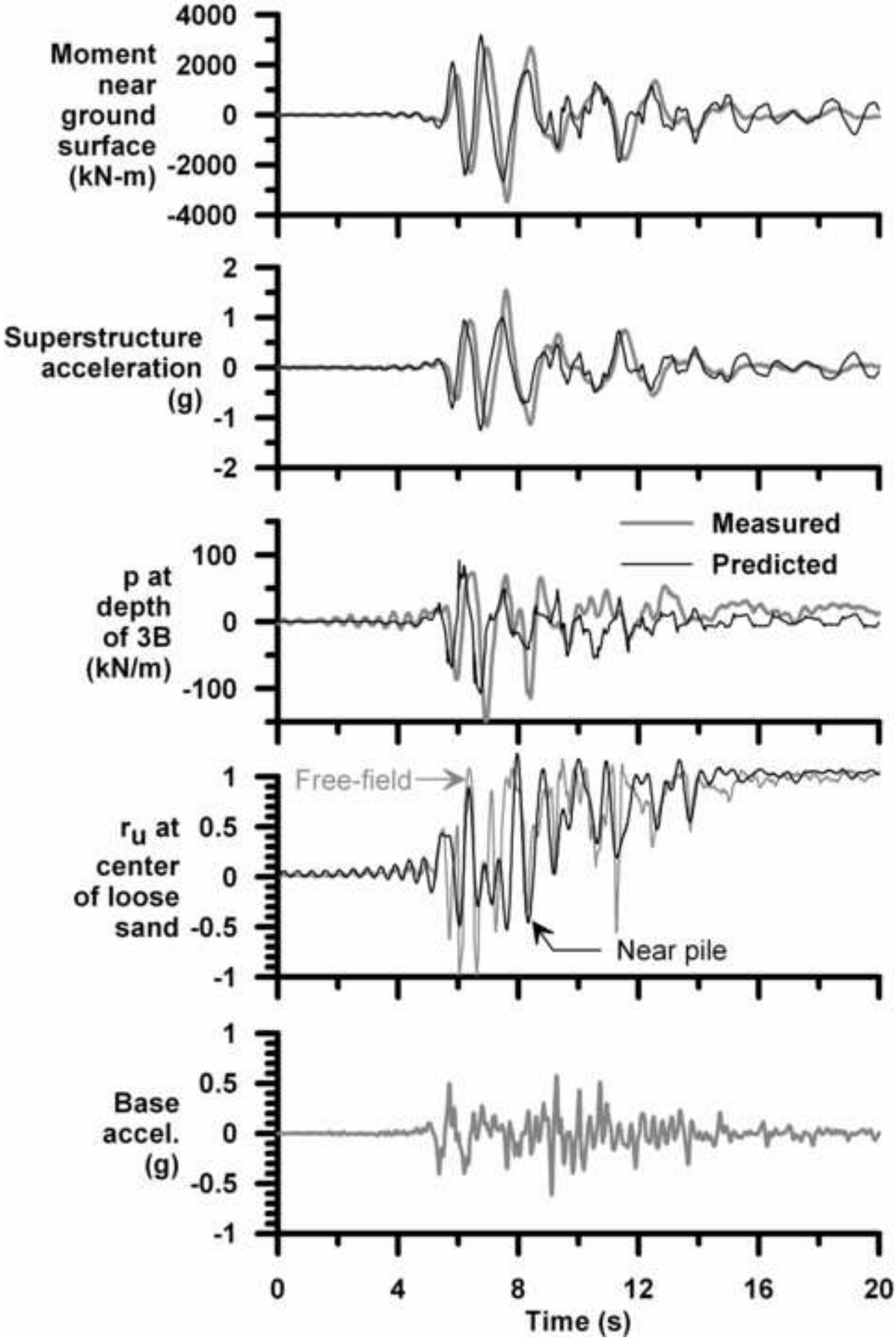

Figure8
Click here to download high resolution image

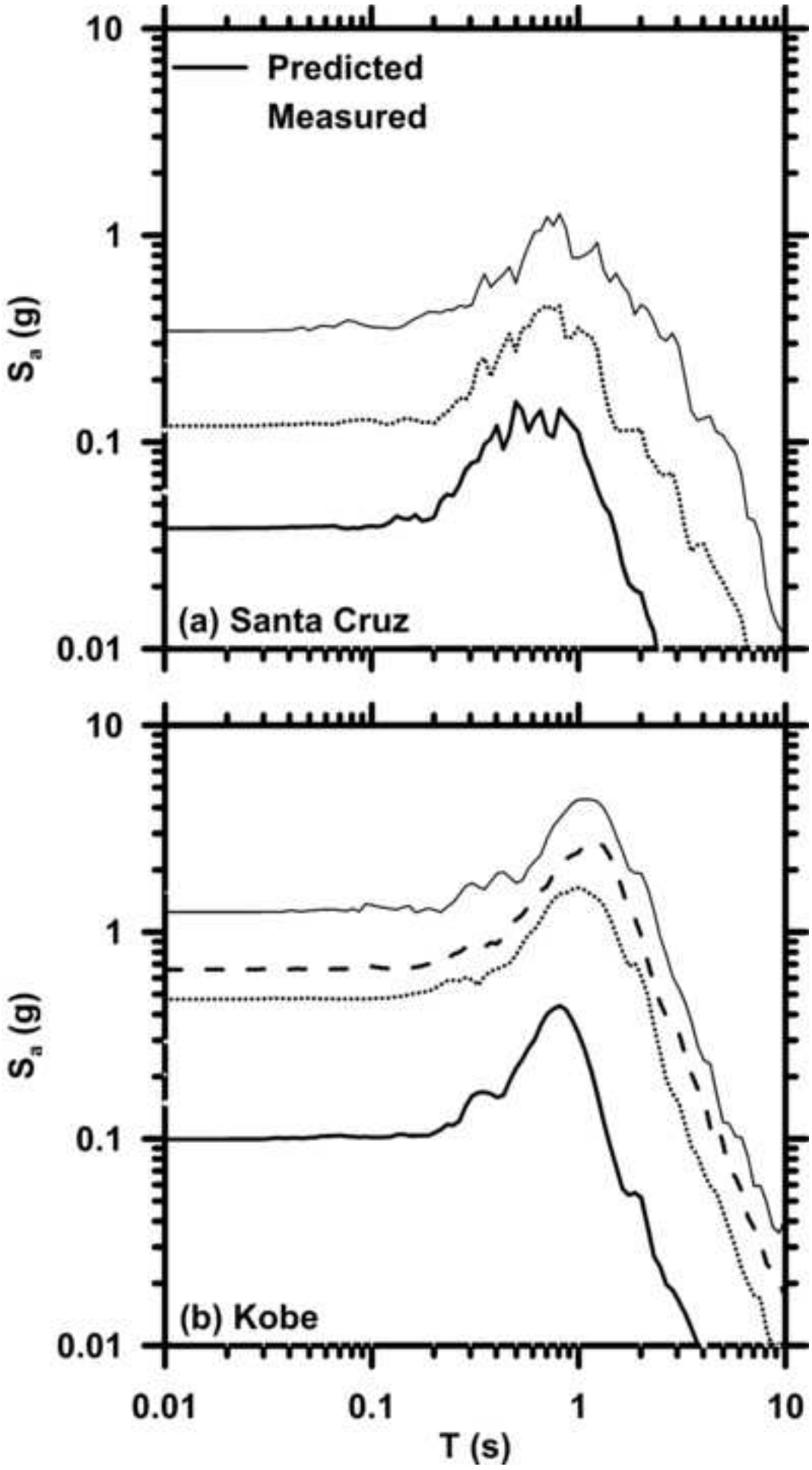

Figure9
Click here to download high resolution image

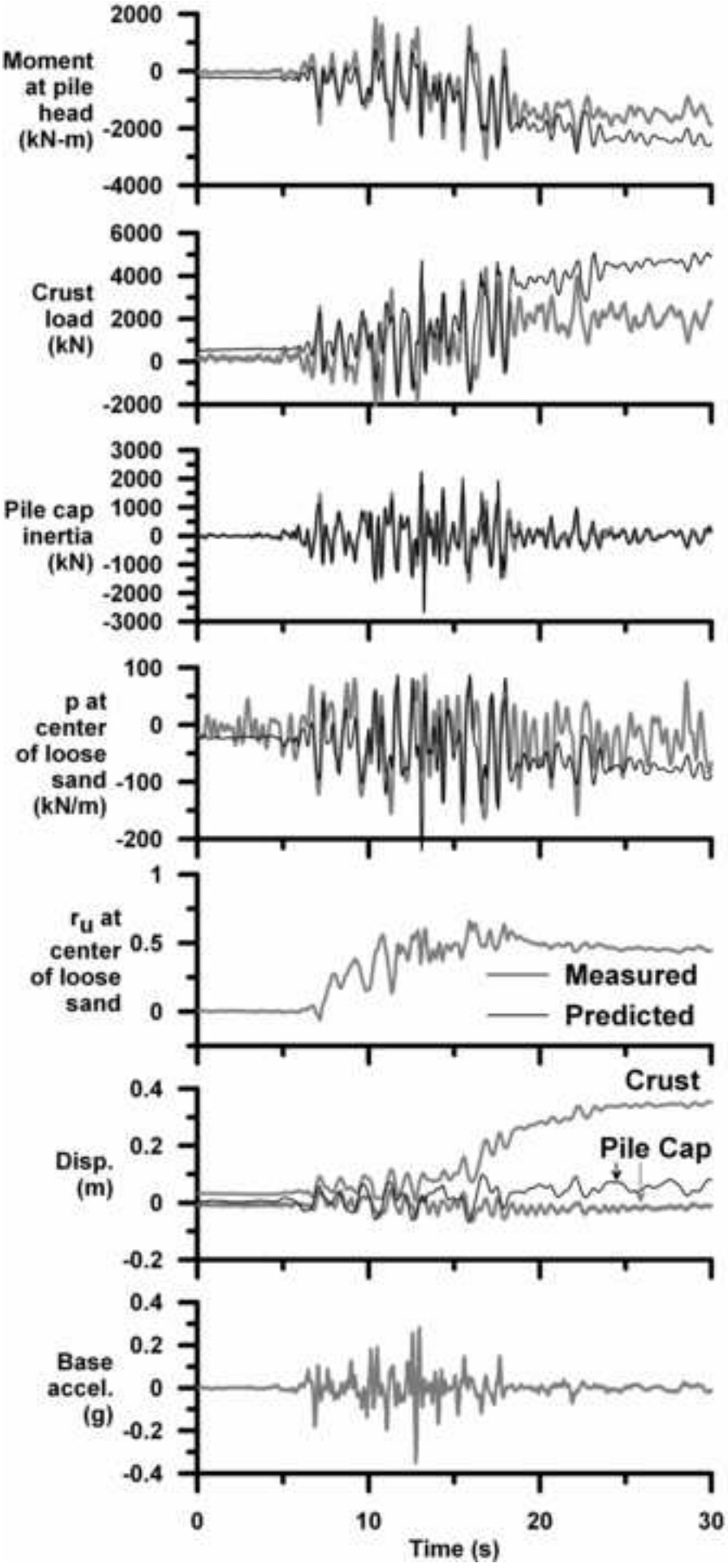

Figure10
Click here to download high resolution image

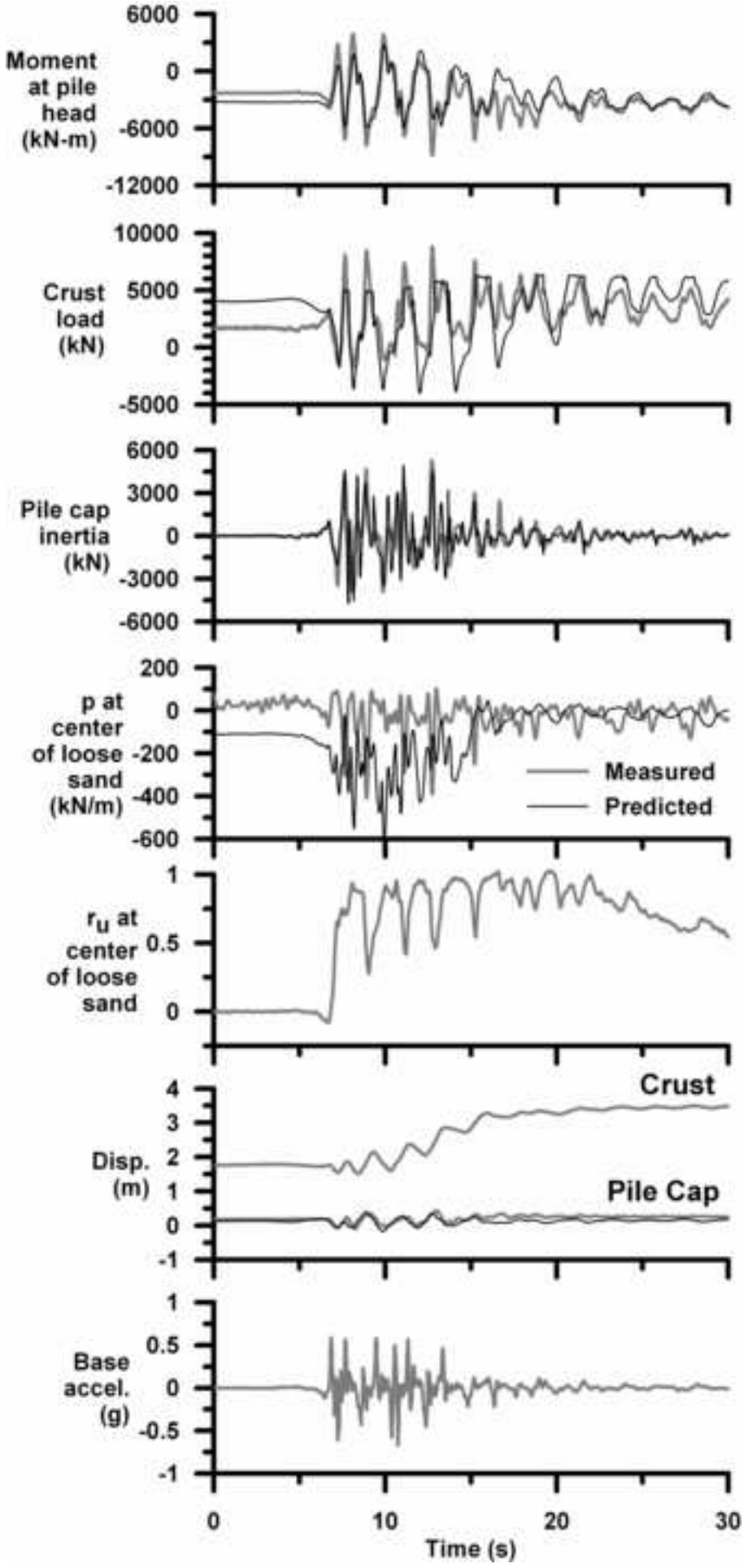

Figure11
Click here to download high resolution image

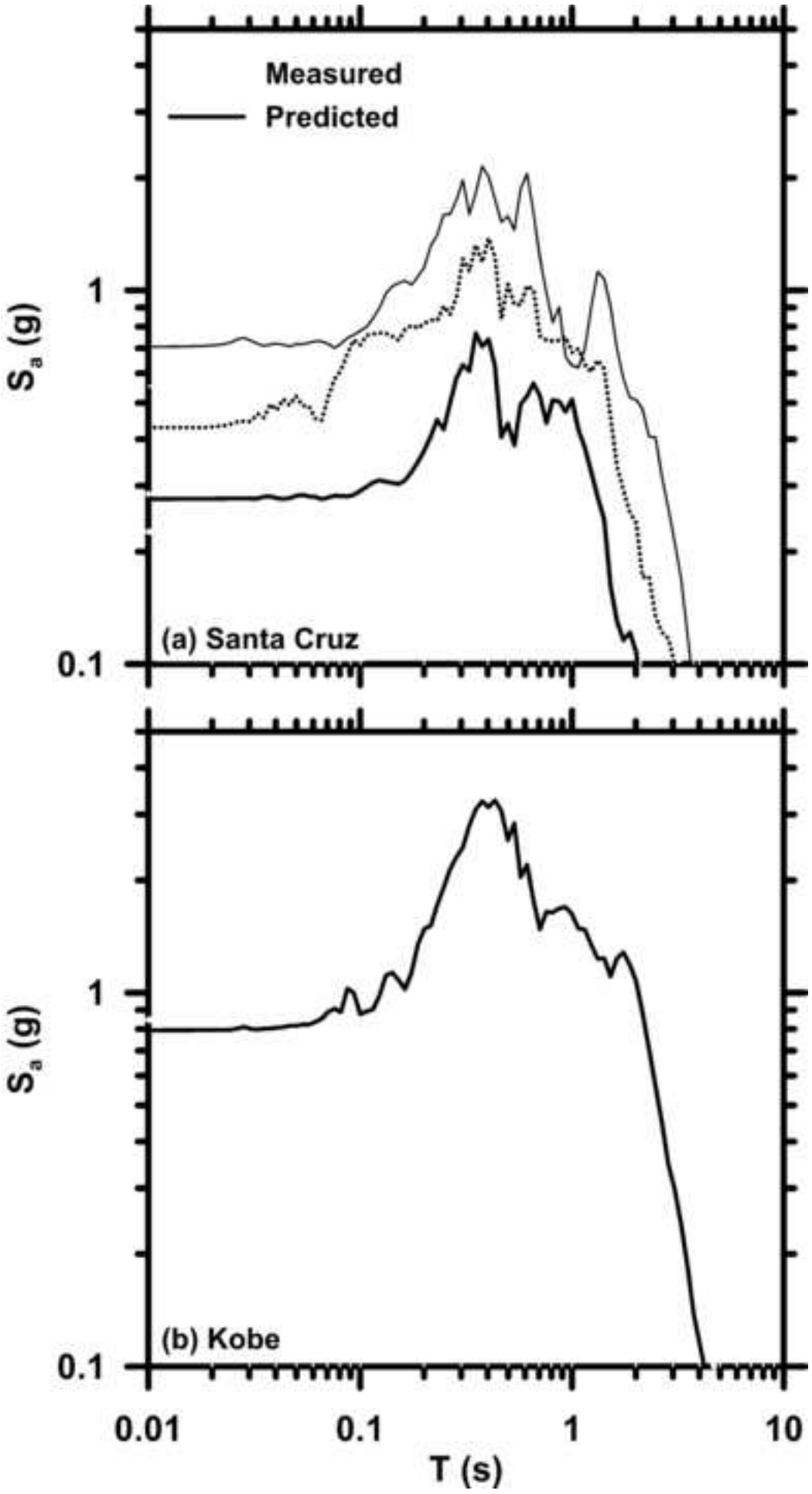

Figure12
Click here to download high resolution image

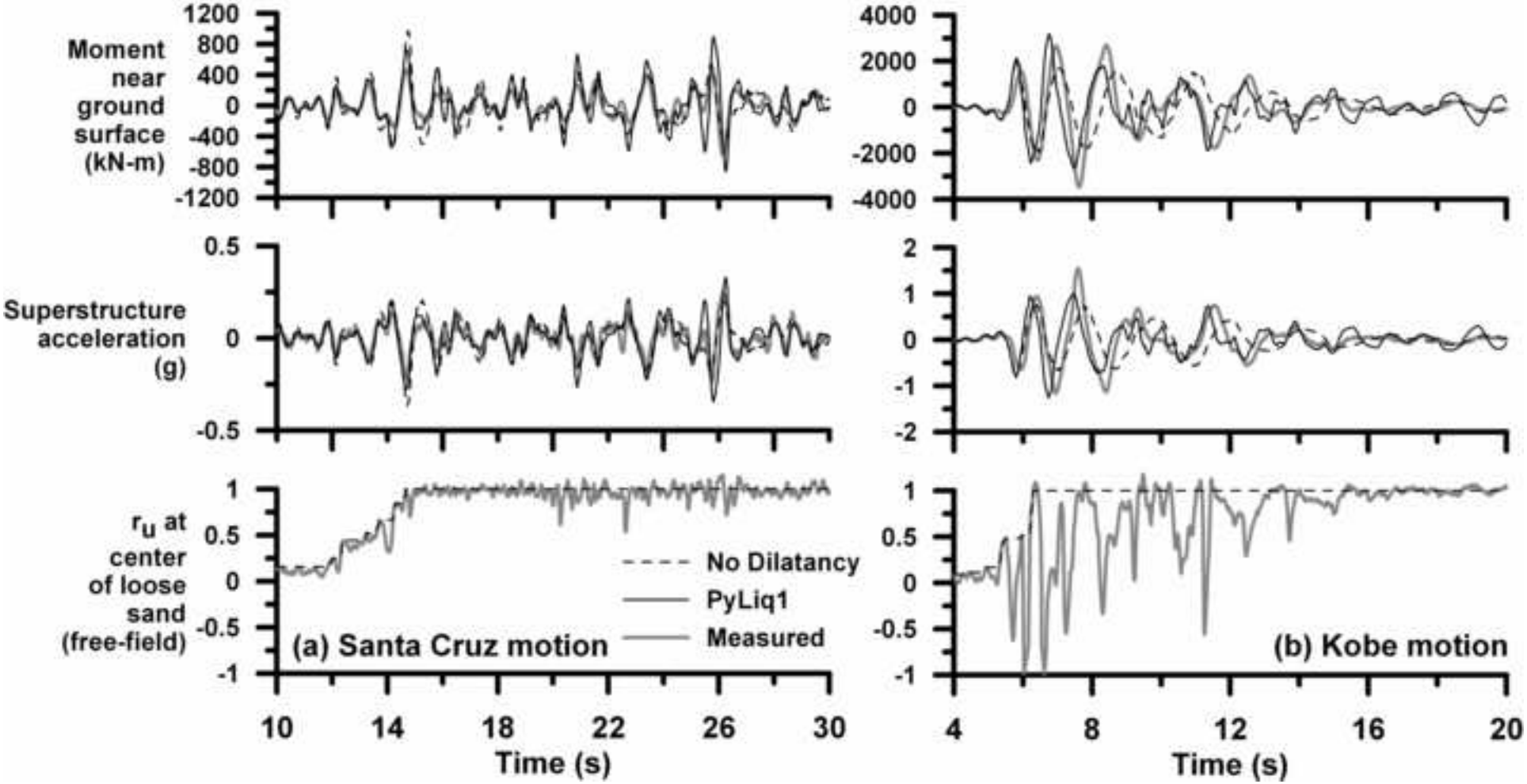

Figure 1. Example p-y behavior for PySimple1 material showing (a) the element configurations, (b) to (e) the contributions of each component, and (f) the overall material response.

Figure 2. Schematic showing ground motion and mean effective stress from site response analysis input to free ends of PyLiq1 elements.

Figure 3. Response of PressureDependMultiYield02 material to cyclic simple shear stress path, and of PyLiq1 material attaching soil element to a rigid pile.

Figure 4. Response of PressureDependMultiYield02 material to cyclic simple shear loading and static shear stress, and PyLiq1 material attached to rigid pile and flexible pile.

Figure 5. Model sketches for centrifuge tests (a) CSP2 and (b) SJB03.

Figure 6. Measured and predicted time series for single pile from test CSP2, Santa Cruz motion "j".

Figure 7. Measured and predicted time series for single pile from test CSP2, Kobe motion "l".

Figure 8. Acceleration response spectra (5% damping) for measured and predicted superstructure motion for test CSP2 for (a) three Santa Cruz motions, and (b) four Kobe motions, of varying intensity.

Figure 9. Measured and recorded time series from test SJB03 for the medium intensity Santa Cruz motion.

Figure 10. Measured and predicted time series from test SJB03 for the large intensity Kobe motion.

Figure 11. Acceleration response spectra (5% damping) for measured and predicted pile cap motion for (a) three Santa Cruz motions of varying intensity, and (b) one Kobe motion.

Figure 12. Influence of dilatancy on pile response is small for (a) Santa Cruz motion and large for (b) Kobe motion.